

POLITECNICO DI TORINO
Corso di Laurea in Ingegneria Energetica e
Nucleare

Final exam



Theoretical and experimental analysis of a solid
adsorption dehumidifier for solar DEC system

CANDIDATE:
Niccolò Alberti

THESIS ADVISOR:
Prof. Marco Simonetti

RESEARCH SUPERVISORS:
Ing. Vincenzo Maria Gentile

GRADUATION YEAR:

2018

Summary

SIMBOLS	c
Subscript	e
ABSTRACT.....	g
1 SOLAR COOLING	1
1.1 Introduction	1
1.2 Technologies	2
1.2.1 Absorption chillers.....	4
1.2.2 Adsorption chillers.....	6
1.2.3 Solid desiccant cooling with rotating wheels	7
1.2.4 Solar DEC	7
1.3 Open cycle solar DEC	7
2 ADSORPTION	13
2.1 Differences between adsorption and absorption	13
2.2 Physical adsorption	13
2.3 Models.....	16
2.4 Van der Waals forces	19
2.5 Electrostatic Energies.....	21
2.6 Capillary condensation.....	22
2.7 Materials and technologies.....	22
3 ENERGY AND EXERGY ANALYSIS.....	27
3.1 Energy analysis	27
3.2 Exergy analysis	29
3.2.1 Equations	30
3.2.2 Performance parameters	35
3.3 Exergy comparison with an heat pump	36

4	EXPERIMENTAL TEST OF THE SYSTEM.....	39
4.1	Test-Rig Description	39
4.2	DAQ and sensor calibration	48
4.2.1	Objective	49
4.2.2	Method	49
4.2.3	Results.....	49
4.2.4	Final equations	53
4.3	Tests	55
4.3.1	Pressure drops	60
4.4	Data analysis	68
5	CONCLUSIONS	72
6	BIBLIOGRAPHY	74
7	WEBLIOGRAPHY FOR FIGURES	76

SIMBOLS

A_c : collector surface [m^2]

b : Langmuir equilibrium constant

c : BET constant

c_p : specific heat [$\text{J}/(\text{kg}\cdot\text{K})$]

COP : coefficient of performance

D : average particles diameter [m]

d : fins distance [mm]

E : energy [J]

E_f : electric field

Ex : exergy [J]

e : specific exergy [J/kg]

ex : exergy flux [J/kg]

G : Gibbs free energy [J]

K : Henry constant

H : enthalpy [J]

h : specific enthalpy [J/kg]

I : irradiance

L : bed thickness [m]

M : molar weight [g/mol]

m : mass [kg]

\dot{m} : mass flow rate [kg/s]

MRC : moisture removal capacity [g/s]

n : max number of layers adsorbed

P_s : pressure of saturation [Pa]

p : fins step [mm]

Q : heat [J]

Q_q : the quadrupole moment

R : universal gas constant [J/(kg·K)]

r : distance between the particles [m]

r_0 : heat of evaporation [J/kg]

r_c : critical radius of capillary

Re : Reynolds number

S : entropy [J/K]

S_b : bed section [m²]

\dot{S}_{gen} : entropy generation [W/ K]

T : temperature [K]

$V(r)$: Lennard-Jones potential

V_a : air velocity [m/s]

v_m : volume adsorbed by the monolayer [m³]

x : absolute humidity [kg/kg]

W : work [J]

\dot{W} : work [W]

α : polarizability

ε : porosity

ϵ : depth of the potential well

η : efficiency

ϑ : coverage fraction

μ : chemical potential [J/mol]

μ_d : the dipole moment

σ : distance at which the potential between particles is zero

σ_w : water surface tension [N/m]

ϕ : atomic interaction

φ : relative humidity

ω : humidity ratio [kg/kg]

$\tilde{\omega}$: mole fraction ratio [Nmol/Nmol]

ρ_a : air density [kg/m³]

Subscript

a: air

ads: adsorption

c: condenser

ch: chemical

cool: cooling

D: dispersion

dew: dew

e: evaporator

el: electric

in: inlet

loss: lost

obt: obtained

out: outlet

P: polarization

p: processed

ph: phisycal

Q: quadrupole

R: repulsive

reg: regeneration

sol: solar

t: total

th: thermic

v: water vapour

wb: wet bulb

μ : field-dipole

0: dead state

ABSTRACT

In the contemporary era energy saving for the domestic air conditioning has become a central point for the development of new technologies. So new systems and phenomena are studied for this application. Consequently also air dehumidification has become a very important air treatment that permit to have good quality air with a lesser energy demand. Classic dehumidification systems has a condensation battery with a compressor for the cooling liquid while new technologies employ adsorption materials to guarantee the air dehumidification with a very low cycle energy cost. These technologies find a good ally in solar cooling systems because they can provide a hot water storage for the regeneration of adsorbent. Is reasonably thinking that the air dehumidification demand and hot water available from solar collector are in phase. There are already tested systems like rotating wheel that have an interesting employ for the open cycle air treatment. Another important aspect is that the same solar system can provide heating for winter and domestic hot water. The most promising application is in climate with humid summer and sunny winter with an high solar radiation. In this study a prototype system is studied. In the laboratory of the Department of energy, Galileo Ferraris, at the Politecnico di Torino a solar DEC wall with a coated zeolite battery has been built. This battery gives the possibility to perform the adsorption with a cooling water system, to carry out the heat of the reaction. The focus of the work is about the study of the second principles efficiency of this new technology compared to a classical system like a heat pump.

1 SOLAR COOLING

1.1 *Introduction*

Today the interest on solar cooling application is on the rise; this is due to the growing demand on cooling energy and for the importance to reduce the greenhouse emission. Augustin Mouchot was a French inventor; he was the pioneer of solar energy research and in 1866 developed the first parabolic trough solar collector and in the 1878 he developed an engine for the Universal Exhibition in Paris [1] (Figure 1).

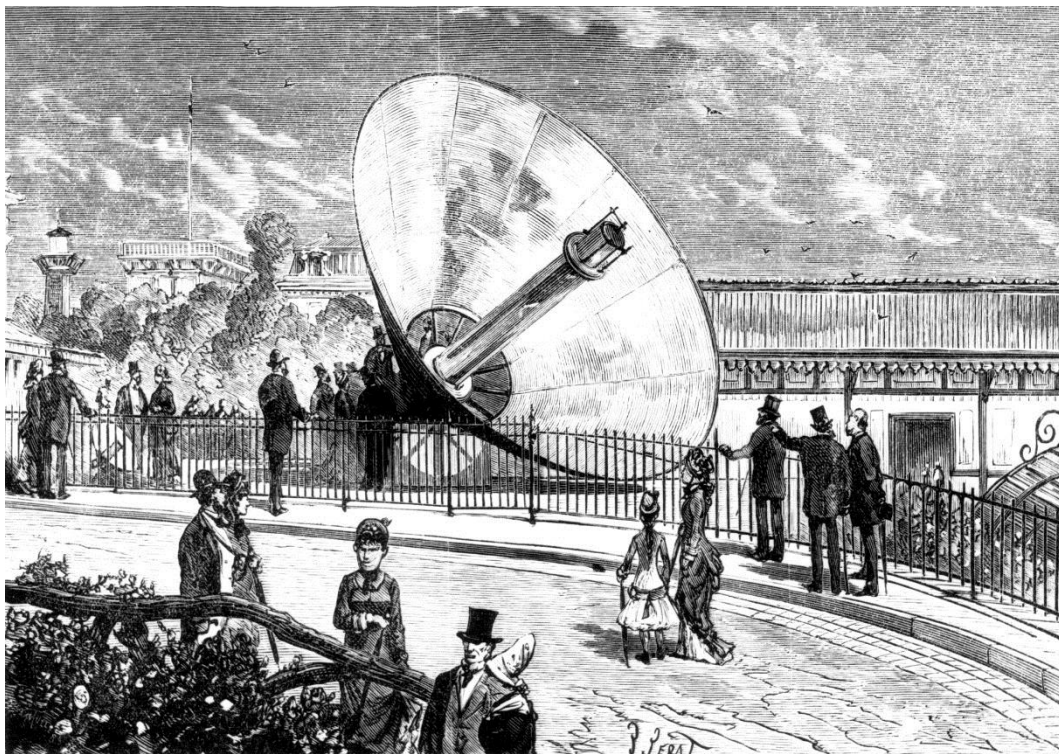


Figure 1 – Universal Exhibition in Paris (1878)

In a solar cooling system the energy of the sun is used to drive the cooling process. The cooling load of a building is the sum of latent and sensible loads [2], and this technology can be very interesting for residential applications thanks to many important characteristics. There is an important saving in consumption of primary energy because the only energy that drive the process is the solar radiation. Accordingly with this there is an important saving in CO₂ emissions. There is also the possibility to have a combined system that provide cooling in summer and heating in winter (air and water). Finally one of the most important

reasons for the interest in this technology is that the cooling demand and solar radiation availability are in phase (Figure 2).

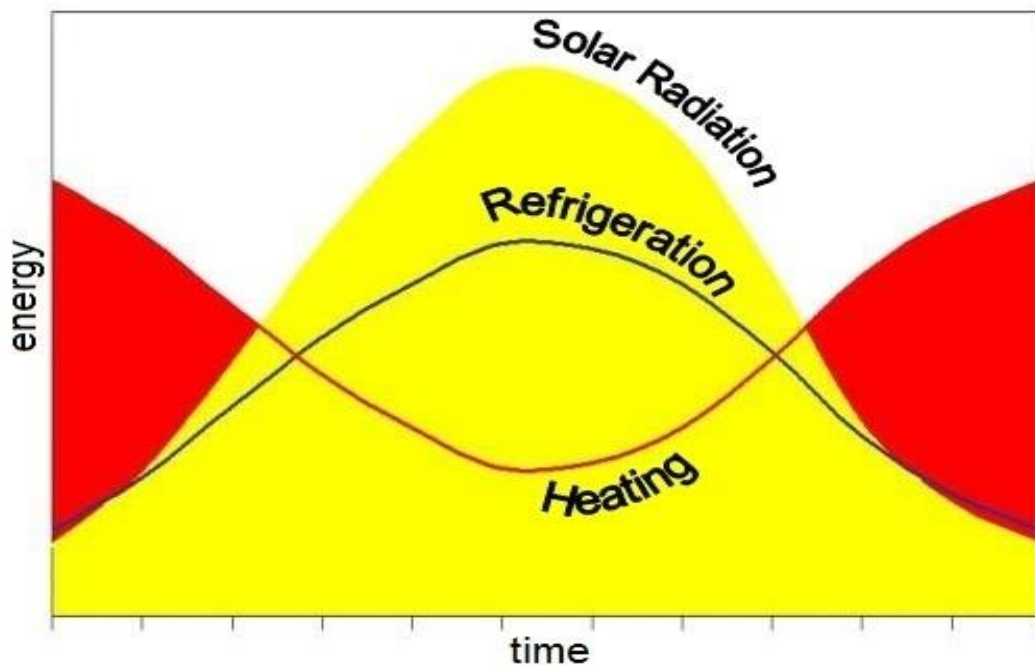


Figure 2 – Time variations of the solar radiation and demands of refrigeration and heating. (source: www.ofrioquevemdosol.blogspot.it)

Solar cooling is a technology that performs differently in different climate regions. It's efficiency is high where is high the efficiency both for solar collectors and for a dehumidification system.

1.2 Technologies

This technology is composed by a typical solar thermal system. It has solar collectors, storage tank, control unit, pipes and pumps, eventually a heat rejection units to expel the waste heat of the cooling process and a thermally driven cooling machine. The solar collectors efficiency is given by the ratio between the power and the product between the solar irradiance and the collectors area:

$$\eta_{sol} = \frac{W}{(I \cdot A_c)} = \frac{W}{Q_s} \quad (1)$$

Then the efficiency of a refrigerant machine is given by the ratio between the cooling power and the work input:

$$\eta_{cool} = \frac{Q_e}{W} \quad (2)$$

So the combination of the two efficiencies became [3]:

$$\eta_{sol-cool} = \eta_{sol} \cdot \eta_{cool} = \frac{Q_e}{Q_s} \quad (3)$$

Thermally driven chillers are characterized by three temperature levels. A high temperature level at which the driving temperature of the process are provided, a medium temperature level at which both the heat rejected from the chilled water and the driving heat have to be removed, and a low temperature level at which the chilling process is operated (Figure 3).

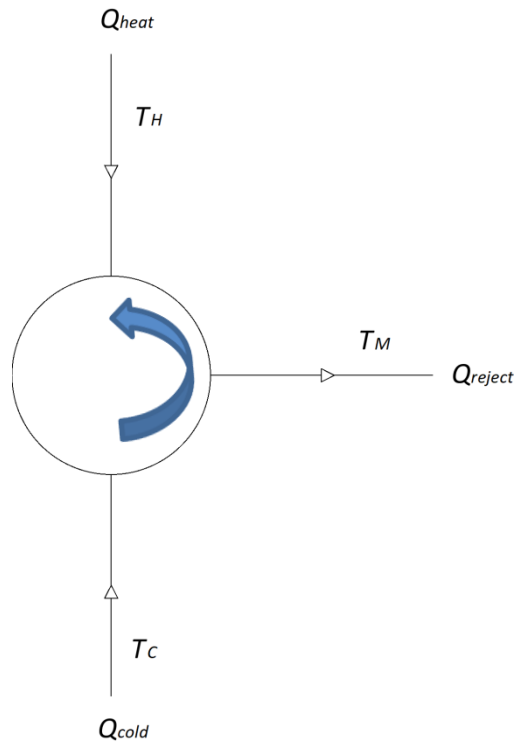


Figure 3 – Scheme of a thermally driven chiller

A chiller has to handle three heat sources during its basic process: Q_{cold} is the heat coming from the delivery and rejected from the chilled water in the evaporator of the chiller (chilling power), Q_{heat} is the required heat for the regeneration and Q_{reject} , the sum of Q_{cold} and Q_{heat} , has to be removed at a medium temperature level T_M . Q_{heat} is delivered either by the solar system or by backup heat sources, e.g. by district heat or by a gas burner. The parameter that describes the efficiency

of a thermally driven chiller is the thermal Coefficient Of Performance (COP_{th}). This is defined as the fraction between heat rejected from the chilled water cycle and the required driving heat. In this definition the electricity consumption is not considered.

$$COP_{th} = \frac{Q_{cold}}{Q_{heat}} \quad (4)$$

The chilled water temperature depends on the installed system and higher temperatures allow to reach higher performance. Solar cooling systems have an higher investment cost than traditional technology; the PBT (Pay Back Time), the period of time required to regain the funds expended in an investment, is considered too long but some national policies support these systems [4].

1.2.1 Absorption chillers

Absorption chillers are the widely used chillers in the world. Often they don't require electrical input and, at the same capacity, they are physically smaller than adsorption chillers [3]. They consist in a compression of the refrigerant by using a liquid refrigerant/sorbent solution and a heat source. This allow to replace the electric power of the mechanical compressor. Typically for air conditioning is used a liquid $H_2O/LiBr$ solution with water as refrigerant. Most system use an internal pump but it consumes a little electric power. During the operation of these systems the solution crystallization has to be avoided by internal control of the heat rejection temperature in the machine. The evaporation of the refrigerant in the evaporator at very low pressure causes the cooling effect. Vaporized refrigerant is absorbed in the absorber, diluting the $H_2O/LiBr$ solution. Heat has been removed to make the absorption process efficient. The solution is continuously pumped into generator, where the regeneration of the solution is achieved by applying heat (hot water). Than the refrigerant leaving the generator condenses thanks to the cooling water in the condenser and circulates by means of an expansion valve again into the evaporator. Typically size, for economic reason, of these chillers are several hundred of kW. The required heat source temperature is usually above $80^\circ C$ for single-effect machines with a COP in the range of 0.6 to 0.8. Double-effect machines with two generator stages require an higher driving

temperature (above 140°C) but reach higher COP (up to 1.2) (Figure 4 and Figure 5).

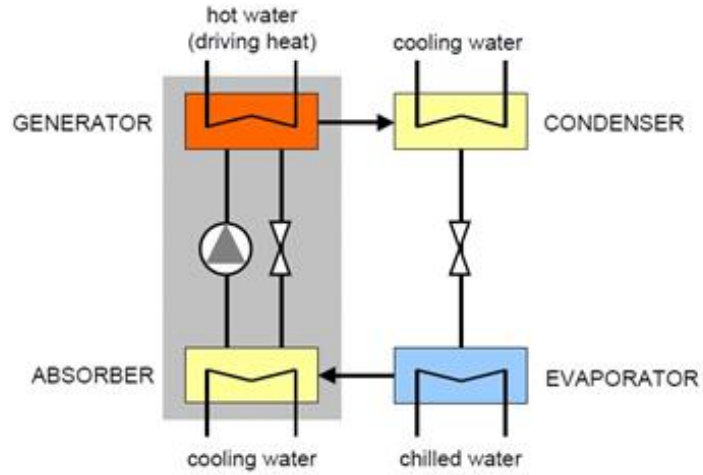


Figure 4 – Absorption process (source: ESTIF, key issues for renewable heat in Europe. August 2006)

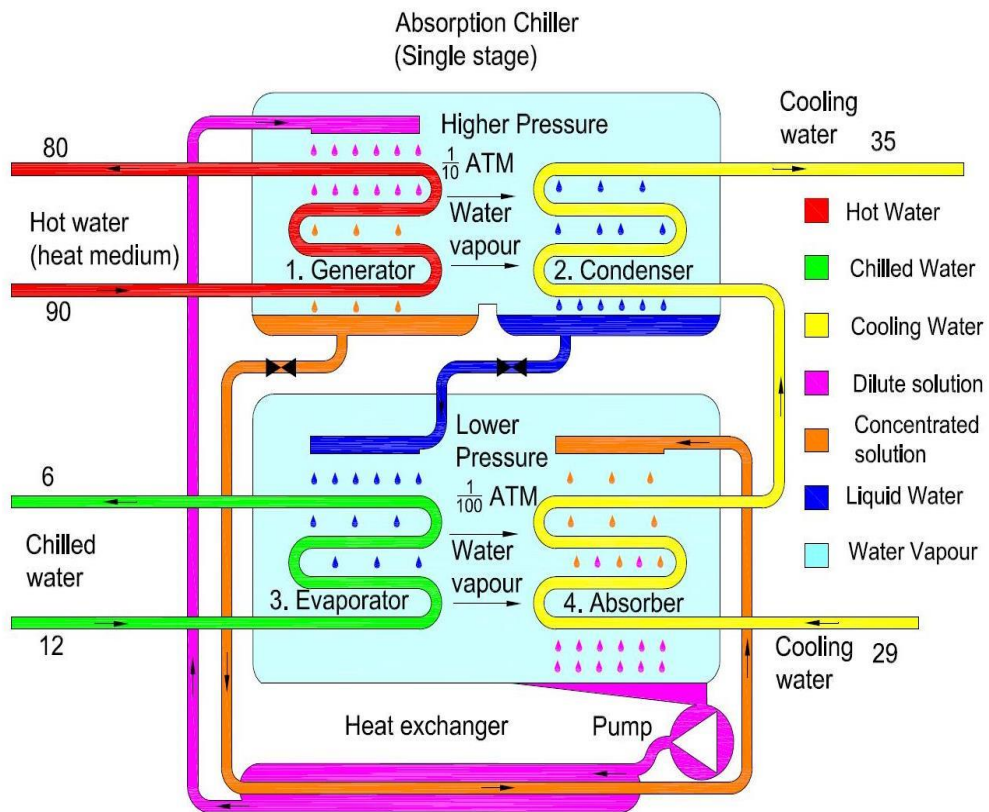


Figure 5 – Absorption process

1.2.2 Adsorption chillers

In these chillers the sorption material is solid. Water is used as a refrigerant and silica gel as a sorbent. Physical adsorbents like zeolite, silica gel and activated carbon can be regenerated by being heated when saturated. The machine consists of two sorbent compartments, one evaporator and one condenser. In the first compartment the sorbent is regenerated using hot water coming from the heat source (e.g. solar collector) while in the second compartment the sorbent adsorbs the water vapour entering from the evaporator. This compartment has to be cooled in order to support a continuous adsorption. The water becomes vapour in the evaporator; the useful cooling effect is produced here. When the sorbent in the adsorber becomes full, the two chambers are switched over. With a driving heat temperature of about 80°C, the system achieved a COP of about 0.6, but it is possible to use also heat source about of 60°C. These systems are mechanically simple and robust. There is no pump, so only a minimal electric power is consumed. A disadvantage is the large volume and weight [3] (Figure 6).

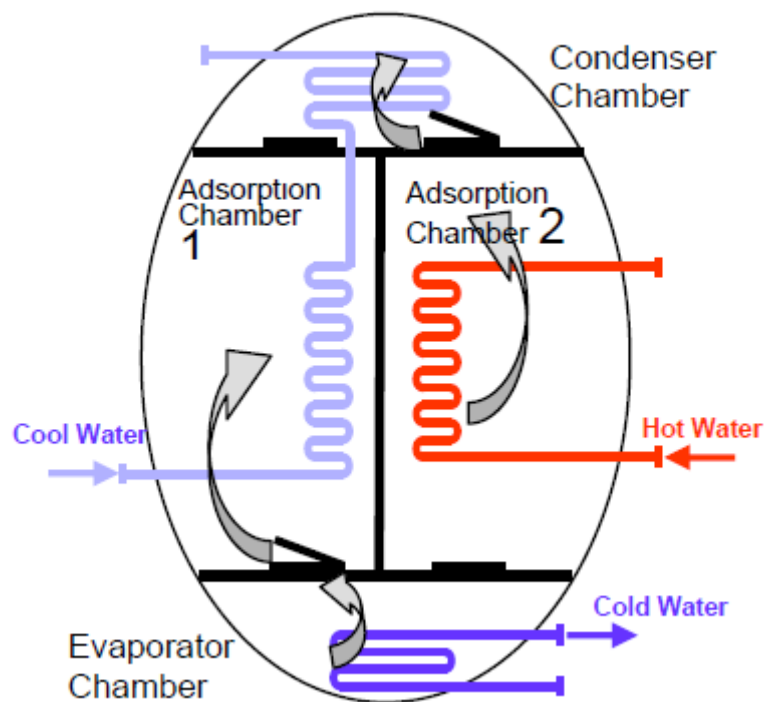


Figure 6 – Adsorption process

1.2.3 Solid desiccant cooling with rotating wheels

These systems can provide conditioned air with an open circuit. Warm and humid ambient air enters in the rotating desiccant wheel and it is dehumidified by physical adsorption. The adsorption process is exothermic so a heat recovery system is needed. This permit a significant pre-cooling of the supply air. Then the air is humidified and cooled according to the desired temperature and humidity of the supply air stream. The exhaust air stream of the rooms is humidified close to the saturation point to exploit the full cooling potential in order to allow an effective heat recovery. This stream is then heated by the heat source (solar thermal systems) and it used to regenerate the desiccant wheel. The range of temperature of heat source is in a comparatively low range from 50°C to 75°C [5].

1.2.4 Solar DEC

Solar DEC (Desiccant, Evaporative Cooling) uses solar collectors to drive the regeneration of the sorbent. These systems may be classified into: closed systems: they provide chiller water that is distributed through a water network to decentralized room installations like fan coils. Open systems: they treat directly external air providing cooled and dehumidified air according to comfort conditions and ventilation requirements. The refrigerant for the cooling is always water because it is in direct contact with the atmosphere. Often a rotating wheel is used with a solid sorbent (e.g. silica gel or zeolites)[5].

1.3 Open cycle solar DEC

Open cycle solar DEC systems uses typically a rotating desiccant wheel, DW, filled with silica gel grains that covered the honeycomb structure as a sort of coating. Air passes through the lower part of the wheel where silica gel grains hold the vapour. The upper part of the wheel is regenerated both from solar collectors and from rejected heat of the chiller when it is present. The base scheme of an open cycle system is composed by the DW, HX thermal recovery, HU that performs the evaporative cooling and a heating coil fed by solar collectors (Figure 7) [6].

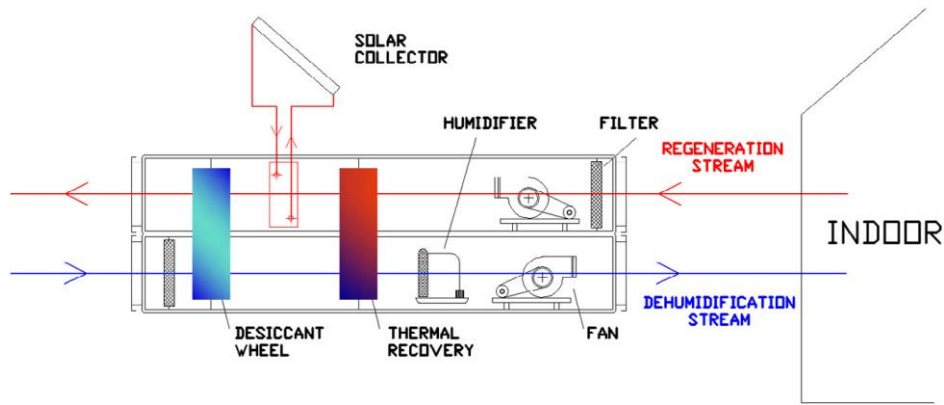


Figure 7 – Open cycle solar DEC

The upgraded layout provides, before the desiccant wheel, a coil, CC1, that is utilized for pre-dehumidify the stream. If the supply air doesn't reach the desired value of temperature with the HX, a second coil, CC2, controls the supply air temperature. HX is a sensitive heat exchanger that transfer the heat from the supply air to the return air after the humidification with HU (indirect evaporative cooling). After the HX there are two heating finned coil. The first, HC1, transfer to return air the heat coming from the heat pump. The second, HC2, heats the stream with the heat coming from the solar collectors. When regeneration air reaches the temperature required to drive the desorption it passes through the DW (Figure 8) [7].

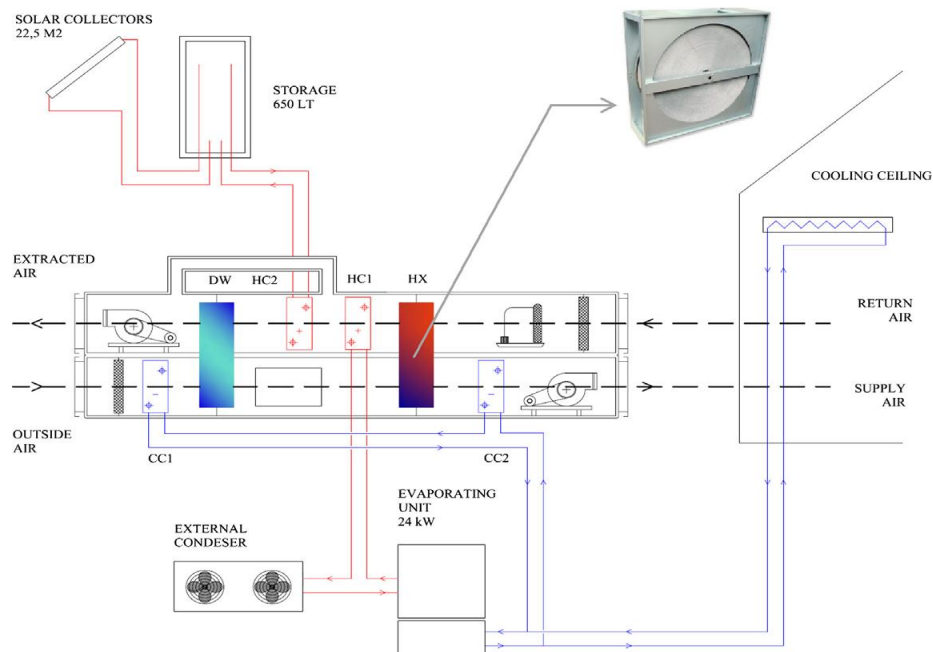


Figure 8 – Open cycle solar DEC with two additional coil

Another type of solar DEC configuration is a modification of this system, carried out from [8]. This configuration presents two wet heat exchangers, HX1 and HX2, in which the evaporative cooling is performed. The layout of this DEC gives the possibility to operate in different MODEs (Figure 9).

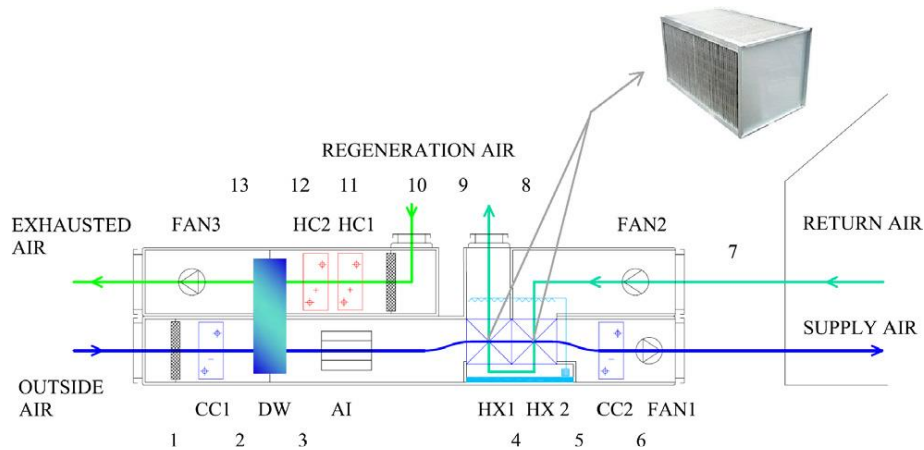


Figure 9 – Open cycle solar DEC with two wet heat exchangers

Wet heat exchanger used for indirect cooling process are composed by several channels. The exchanger is an air to air exchanger (Figure 10) where the return air from the room passes through the wet channels sprayed by nozzles, such that a water film evaporates cooling down the surface. The supply air passes through the other side of the channels and cools down [8] (Figure 11).



Figure 10 – Air to air heat exchanger (source: Recuperator)

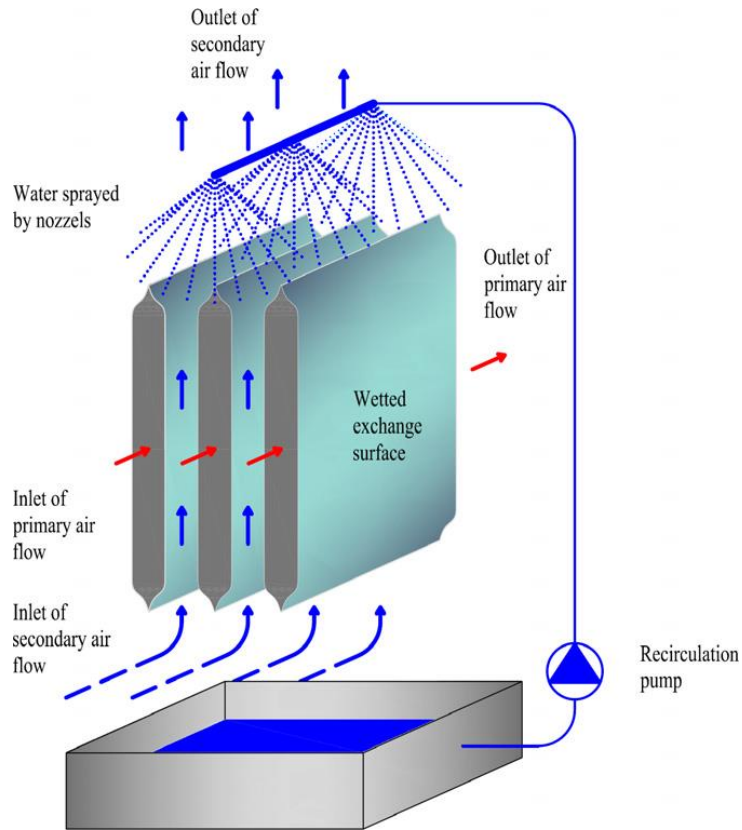


Figure 11 – Evaporative cooling

In [9] is proposed a solar DEC system with a NAC-wall system (Figure 12). The main concept is that the two air flows are driven by only natural convection. It is built a module called NADEH in vertical configuration. This module is subdivided in two chambers working intermittently. When one chambers adsorbs the humidity coming from the environment, the other regenerates the zeolitic battery. After this system that substitutes the desiccant wheel there is an heat exchanger air to air and a evaporative cooling. The regeneration is done with a solar collectors system [9]. The investigation in natural convection technology shows the necessity of further development and optimization, particularly for the adsorption phase [10].

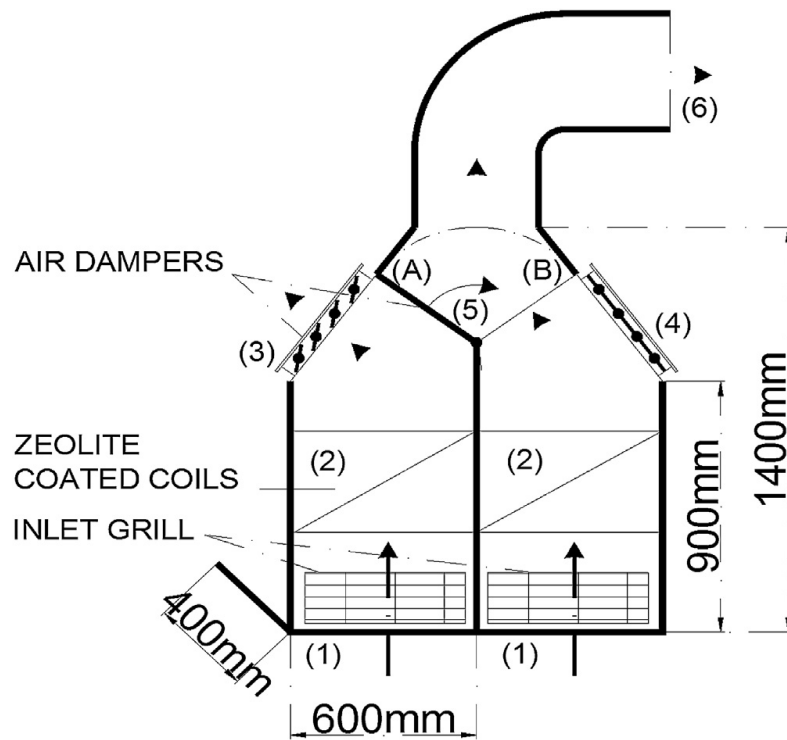


Figure 12 – NADEH wall

In [11] is analysed and monitors a solar Desiccant an Evaporative Cooling (DEC) system working with the freescoo technology installed at the UNIPA in Palermo. The heat exchanger is filled with fine grains of silica gel and is cooled by water flowing through the tubes. There is a 4-way valve that provides the changing of the adsorption bed in order to guarantee the continuity of dehumidification. Results show a clearly energy saving potential in comparison to the conventional technologies. [12]

2 ADSORPTION

2.1 Differences between adsorption and absorption

Porous materials are very interesting for the humidity control on indoor spaces thanks to their capacity to bring water vapour. Performances of a porous material are described by the adsorption isotherms. This curve is a relation at a given temperature between the mass adsorbed and the relative humidity; the latter is defined as the ratio between the vapour partial pressure and the saturation pressure at the same temperature.

Before to start to treat the adsorption phenomena it is important to give a clarification of differences between absorption and adsorption. Absorption, also said chemical adsorption, is a chemical bond. Electron transfer leading to bond formation between sorbate and surface. The heat associated to absorption is high (> 2 or 3 times latent heat of evaporation) and it is a monolayer process. It is often an irreversible interaction in which is necessary to have a substance that can react with the substance to remove. Adsorption, also said physical adsorption, is a van der Waals interaction. There is not electron transfer although polarization of sorbate may occur. Adsorption is characterized by a low heat of adsorption (< 2 or 3 times latent heat of evaporation) and it can be monolayer or multilayer. It is only significant at relative low temperature. The process needs the transport of the substance that will be removed from the flux near to the sorbent surface in order to reach the minimum distance needed for the activation of van der Waals forces. Phenomena are rapid and reversible. This is only a surface phenomenon so the sorbent surface has to be very high for the adsorption efficiency. For this reason the use of material with high level of porosity is recommended. [13]

2.2 Physical adsorption

Physical adsorption is a surface interaction characterized by van der Waals interactions and electrostatic interaction. The first contribution is always present while the second only when the adsorbent have an ionic structure (e.g. zeolite). The fundamental parameters that control adsorption are: exposed surface, total pores volume and pores diameter. The heat of adsorption gives the measure of the strength of the bonding between the sorbent and the sorbate. The process is exothermic. This is correlated to the freedom of sorbate particles that is always

less than the gas phase molecule. In fact the adsorbed molecule has at most two degrees of freedom and the rotational freedom of an adsorbed particle must always be less than that of the gas phase. For this reason the entropy difference related to the phenomenon is always negative during adsorption:

$$\Delta S = S_{ads} - S_{gas} < 0 \quad (5)$$

However, also the Gibbs free energy must be negative, then for the following equation:

$$\Delta G = \Delta H - T\Delta S$$

ΔH must be negative. This is the explanation because adsorption processes are always exothermic [13]. However when the sorbate molecules are small and dipolar (e.g. H₂O and NH₃), the electrostatic contribution become very large, causing an increase of the heat of adsorption. In a physical adsorption process there is no change in molecular state on adsorption (i.e., no association or dissociation). For adsorption on a uniform surface at low concentration that permit to all molecules to be isolated from their nearest neighbours, the equilibrium relationship between fluid phase and adsorbed phase concentration is linear. Henry's law is associated to this linear relationship. The Henry constant may be expressed in terms of pressure or concentration:

$$q = Kc \quad (6)$$

$$q = K'p \quad (7)$$

Brunauer have classified the physical adsorption isotherms into five classes (Figure 13). These curves represent the characteristics of the adsorption process. From a qualitative analysis on an adsorption isotherm is possible to acquire information about the porous material. For examples the isotherms for microporous adsorbent are normally of type I. This behaviour is due to the pore size that is similar to the molecular diameter of the sorbate molecule. Isotherms of type I are typically associated to zeolite adsorbent [13].

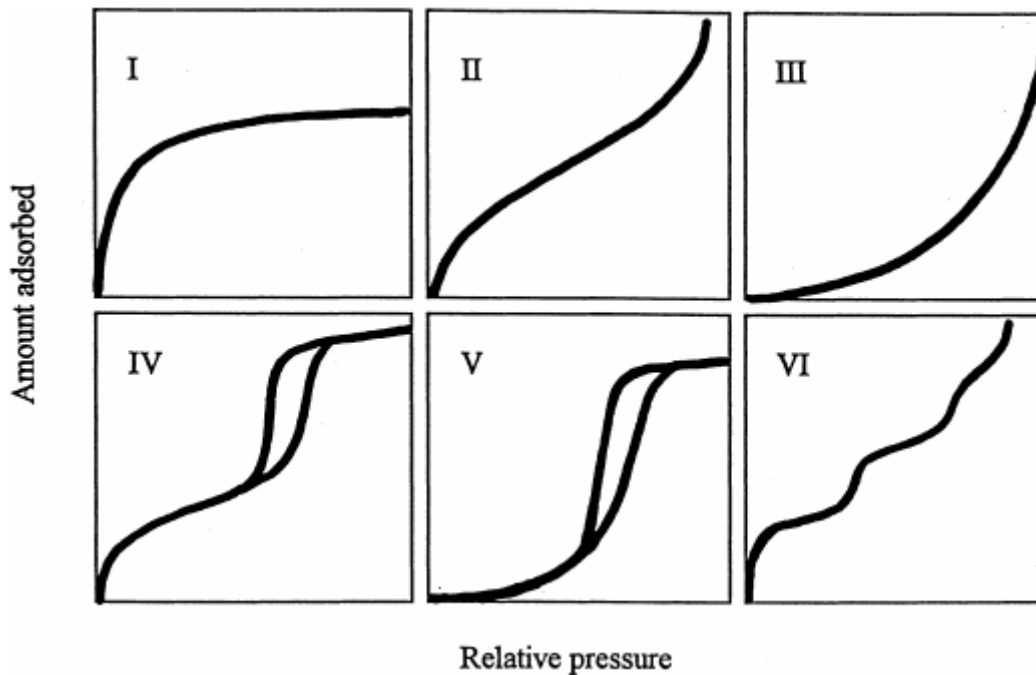


Figure 13 – Adsorption isotherms proposed by Brunauer

Type I: in the first part there is adsorption but after the flex it stops even if the partial pressure increase.

Type II: this curve is typical for macro-porous and non-porous materials. After the saturation of the first layer with the increase in partial pressure the new layer act as the surface for the formation of a second layer.

Type III: not very common. It doesn't show the point with the formation of the layer.

Type IV: a hysteresis cycle is present. Pore blocking phenomena and vapour condensation on capillaries are associated to it. As in type II there is the formation of the first layer and of the second layer.

Type V: as type III is not very common. It is similar to type III but it presents a hysteresis cycle.

Type VI: this type has steps slope. Single steps are the fill of single layers while plateau show when nothing is adsorbed.

Behaviours of adsorption and desorption in a porous media are generally governed by transport within the pore network. So is convenient to consider particles transport as a diffusive process in accordance with Fick's first equation:

$$J = -D(c) \frac{\partial c}{\partial x} \quad (8)$$

But diffusion phenomena may occur by several different mechanism: chemical potential, sorbate concentration, pores dimension and other condition. Particles adsorbed in micro-pores, as in zeolite, never escape from the force field of the adsorbent surface and the transport is promoted to a process that involve jump between adsorption sites [13].

2.3 Models

There are not any theories that describes correctly from a mathematical point of view an experimental isotherm during the hole $\frac{P}{P_0}$ axis interval. There were formulated many empirical equation for the different intervals and many standard isotherms for different materials are obtained.

Langmuir gave a simple theoretical model for monolayer adsorption. The model is based on four basic assumptions:

- The adsorption of molecules takes place at a fixed number of well-defined localized sites.
- Each site can accept one adsorbate molecule.
- All sites are energetically equivalent.
- There is no interaction between molecules adsorbed on neighbouring sites.

For the equation derivation an equilibrium relation is considered:



From the definition of the equilibrium constant K and considering the reactants concentration is obtained:

$$K = \frac{[AB]}{[A][B]} \quad (10)$$

$[AB]$ represents the occupied fraction ϑ of the solid surface, $[B]$ is proportional to the vacant sites equal to $(1 - \vartheta)$ and $[A]$ is proportional to the gas partial pressure. With these assumptions is possible to define the Langmuir equilibrium constant:

$$b = \frac{\vartheta}{(1 - \vartheta)P} \quad (11)$$

The adsorption process is spontaneous and exothermic, so the heat of adsorption is always positive. Then it is possible to evaluate the coverage fraction:

$$\vartheta = \frac{bP}{1 + bP} \quad (12)$$

b is the Henry constant and for low coverage the equation became:

$$\vartheta(p, T) = \frac{b(T)P}{1 + b(T)P} \approx b(T)P \quad (13)$$

For low coverage the relation gives correctly the Henry's law. This is the simplest theoretical model originally developed to represent adsorption on a set of distinctive adsorption sites. In a porous adsorbent there is a continuous progression from multilayer adsorption to capillary condensation in which the smaller pores become completely filled with liquid sorbate. This occurs because the saturation vapour pressure in a small pore is reduced, in accordance with the Kelvin equation, by the effect of surface tension. An important concept on adsorption process is the inversion temperature. This temperature is higher than the temperature during the adsorption and lower than the temperature needed to desorb the sorbent (Figure 14).



Figure 14 – Scheme of inversion temperature

With this temperature it is possible to evaluate the enthalpy difference between before and after adsorption:

$$\Delta G = \Delta H - T^* \Delta S = 0 \quad (14)$$

$$\Delta H = T^* \Delta S \quad (15)$$

During the adsorption heat must be removed while during regeneration heat must be provide [14]. For this is necessary to minimize the regeneration temperature and so the exergy demand. For multi-layers adsorbents there are many theory. BET theory is one of each. For BET theory Van der Waals forces, London interaction in particular, are the cause of adsorbent phenomena. Each molecule in the first adsorbed layer is considered to provide the location for the following adsorbed layer [13]. The BET equation for a multi-layer adsorption is the following:

$$v = \frac{v_m c x}{1 - x} \cdot \frac{1 - (n + 1)x^n + n x^{n+1}}{1 + (c - 1)x - c x^{n+1}} \quad (16)$$

With:

v_m : volume adsorbed by the monolayer

c : BET constant

n : max number of layers adsorbed

These three parameters are evaluated from experimental data. This equation fits correctly the isotherms of type II and III.

Another model is the potential theory, formulated by M.Polanyi. the theory is based on the concept that a gas in contact with a porous surface shows an attraction force. The formation of different particles layers causes the different compression level between each other. The potential equation is formulated as the energy needed to bring a gas molecule from the gas phase to that point:

$$\varepsilon_i = \int_{\delta_x}^{\delta_i} V dp \quad (17)$$

For the evaluation of this integer two main hypothesis considered: the ideal gas law and the incompressibility of fluid. The isotherms that come from this theory are quite good for the interpretation of isotherms of type IV and V. Dubinin proposed an empirical forms of the potential:

$$V = V_0 e^{-k \left(\frac{\varepsilon^2}{\beta^2} \right)} \quad (18)$$

Where V_0 is the limit value of adsorbed volume of the mono-layer, k is a constant and β is the affinity coefficient.

2.4 Van der Waals forces

Van der Waals forces are distance-dependent forces between atoms or molecules. They are not the result of chemical bond, they are weaker than ionic or covalent bond of two order of magnitude. Being weaker than ionic does not means that they are negligible, and in nature there are example of its applications. Animals like Gecko uses these types of interaction to walk on vertical surface; this is possible thanks to an higher number of hair-like structure beneath the toes (setae) that frequently branch several times. The ends of setae are in strictly contact with the surfaces on which geckos climb, generating the interactions [15] (Figure 15).

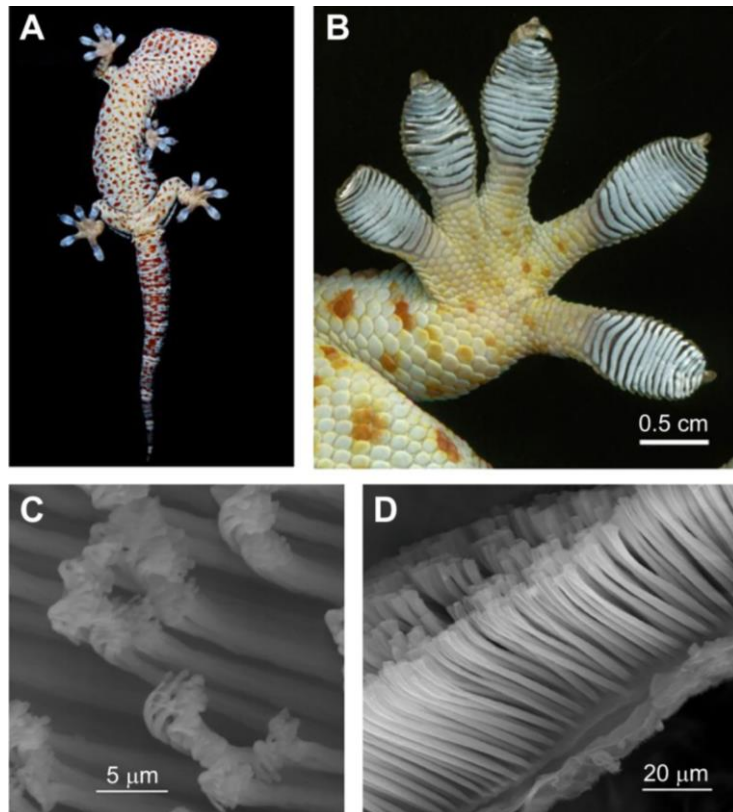


Figure 15 – Toes and setae of gecko

They can be repulsive or attractive depending from the particles charge and from the distance of atoms [13]. Van der Waals forces includes three different interactions:

- Keesom interaction: electrostatic forces that can be attractive or repulsive. This interaction is between two permanent dipoles.

- Debye interaction: force between a permanent dipole and an induced dipole.
- London dispersion interaction: attractive interaction between two induced dipoles

The attractive potential between two isolated molecules correlated to dispersion forces is:

$$\phi_D = -\frac{A_1}{r_{12}^6} - \frac{A_2}{r_{12}^8} - \frac{A_3}{r_{12}^{10}} \quad (19)$$

Where r_{12} is the distance between the centres of the two molecules and A_1, A_2, A_3 are constants. The first terms is always dominant and it is correlated to instantaneous induced dipoles. The repulsive interaction is represented semi-empirically by:

$$\phi_R = \frac{B}{r_{12}^{12}} \quad (20)$$

Neglecting the higher order contribution of the first equation, and combining it with the second, leads to the Lennard-Jones potential equation.

$$V(r) = 4\epsilon \left[\left(\frac{\sigma}{r} \right)^{12} - \left(\frac{\sigma}{r} \right)^6 \right] \quad (21)$$

where:

- ϵ is the depth of the potential well
- σ is the distance at which the potential between particles is zero
- r is the distance between the particles

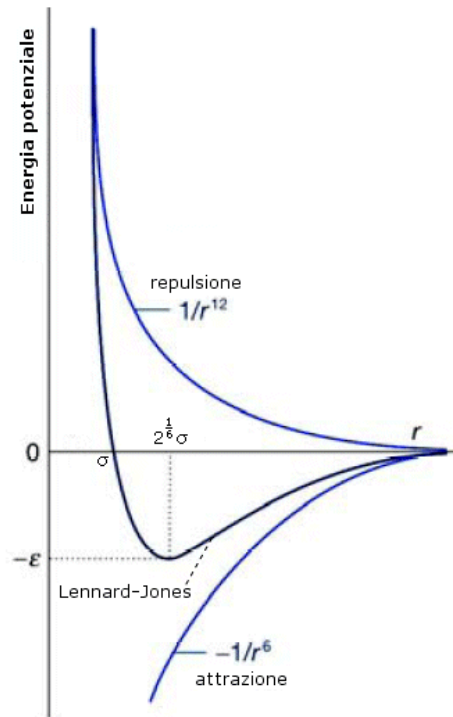


Figure 16 – Lennard-Jones potential

There is a potential well from where the atom falls. This is the equilibrium distances between the two atoms (or molecules) [13].

2.5 Electrostatic Energies

Electrostatic energies are significant only when the adsorbent material has an ionic structure. This is the case of zeolite as adsorbent. In particular when the adsorbed substance is a dipolar molecule, like water, this contribute may be very large and relevant. This phenomenon leads usually to a high heat of adsorption. So the electrostatic potential can be expressed as the contribution of three different potentials: polarization (ϕ_P), field-dipole (ϕ_μ) and field gradient quadrupole (ϕ_Q) interaction [13].

$$\phi_P = -\frac{1}{2} \alpha E_f^2 \quad (22)$$

$$\phi_\mu = -\mu_d E_f \quad (23)$$

$$\phi_Q = \frac{1}{2} Q_q \frac{\partial E_f}{\partial r} \quad (24)$$

With:

E_f : electric field

α : polarizability

μ_d : the dipole moment

Q_q : the quadrupole moment

In conclusion for an ionic adsorbent the overall potential became:

$$\phi = \phi_D + \phi_R + \phi_P + \phi_\mu + \phi_Q + \phi_s \quad (25)$$

Where ϕ_s is the contribution of sorbate-sorbate interaction.

2.6 Capillary condensation

The capillary condensation is the phenomenon that drives the adsorption in porous materials. This happens because the vapour pressure over a curve meniscus, a negative curve, is different from the vapour pressure over a flat water surface. More the capillaries are thin more the menisci are curved and lower will be the vapour pressure inside them. If the air vapour pressure is greater than that inside the meniscus there is a condensation. So there is a continuous progression from multi-layer adsorption to capillary condensation. The pores diameter is a parameter that influences the start point of the phenomenon. The Kelvin equation expresses the pressure at which the capillary condensation starts:

$$\ln \frac{p}{p_0(T)} = \frac{2\sigma_w V_m}{r_c RT} \quad (26)$$

With:

σ_w : water surface tension

V_m : water volume

r_c : critical radius of capillary

R : universal gas constant

2.7 Materials and technologies

There are different types of materials that can be used to dry air from humidity.

Silica gel is a granular, vitreous and porous form of silicon dioxide that can be synthesized both with the polymerization of silica acid that with the aggregation of colloidal silica particles. Water pass through the tiny passage between grains ad it has be adsorbed. Silica gel is simply to regenerate and it is used in rotatory wheels and in heat exchangers. In [16] is demonstrated that the size of adsorbent grains influenced the adsorption and desorption dynamics. It is an high performance adsorbent material but it presents a quite linear adsorbent isotherms without any rapid variation. The regeneration temperature is lower than zeolite and isotherms are of type IV, showing a continuous increase in loading with water vapour pressure. When the pressure increases the layer surface adsorption merges into capillary condensation. Capillary condensation happens in pores of increasing diameter with the increase of pressure. The ultimate capacity of silica gel, at least at low temperature, is generally higher than other solutions (Figure 17).

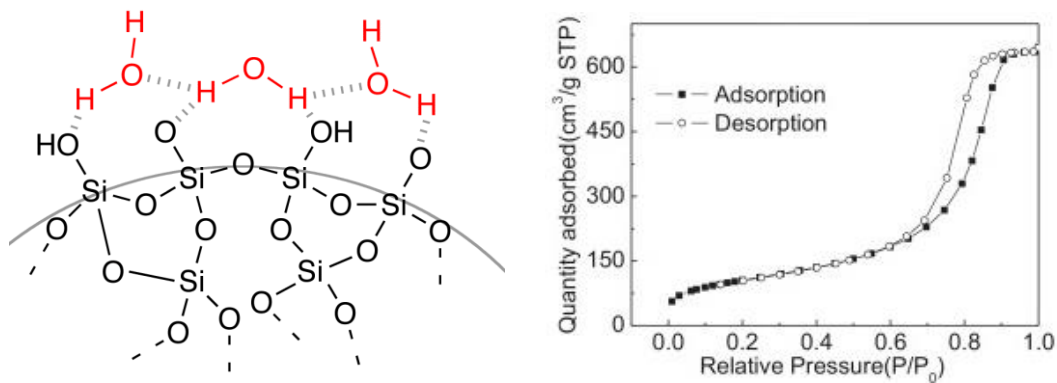


Figure 17 – Molecular structure and isotherms of silica gel

Zeolite is a micro-pores material with a huge number of very small and uniform holes that trap the water molecule when the humid air pass through them. Zeolites have a very interesting capacity to desorb water to air, leaving air with extremely low PPMv level (<100 ppm (%RH)). These materials are more difficult to regenerate than silica gel and isotherms are of type I as it is possible to see in the figure; there is a well-defined saturation plateau corresponding to complete filling of micro-pores (Figure 18).

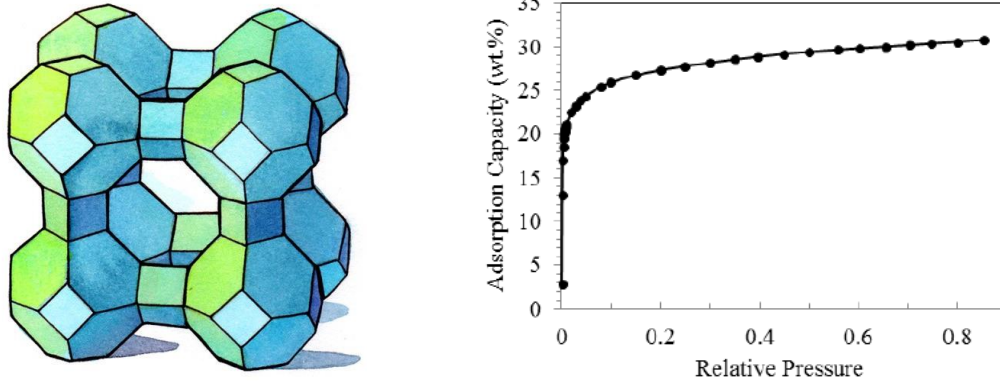


Figure 18 – Molecular structure and isotherms of zeolite

Activated alumina is manufactured from aluminium hydroxide and it is also used as a filter of fluoride, arsenic and selenium. It is characterized by an high surface-area-to-weight ratio. The release is not many difficult.

There are many different solutions to build an adsorbent bed; the most common is used in rotating wheels and consist in filling the space between matrix channels with grain of for example silica gel (1.3) (Figure 19). It is also possible making a thick layer of adsorbent material (e.g. silica gel, zeolite) directly on the channel surface.

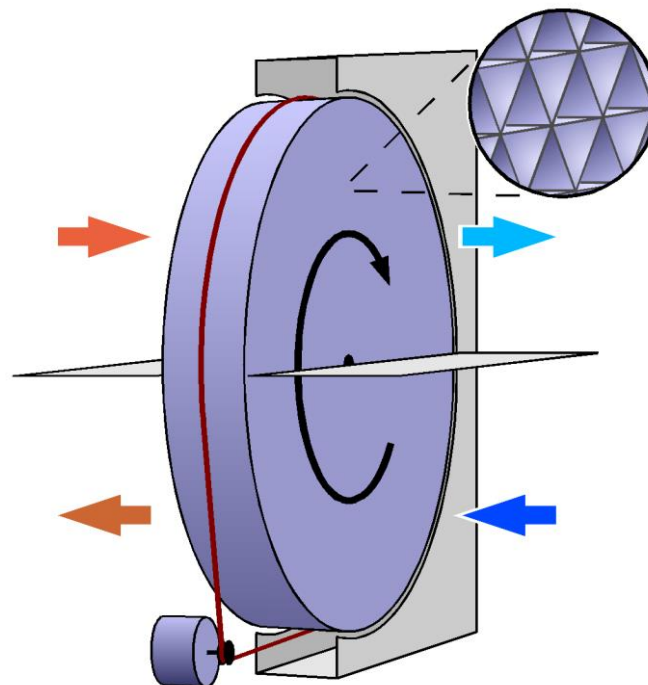


Figure 19 – Rotating wheel with honeycomb structure

In [17] has been studied the best shape of coated channels and find that the best shape is the circular. This tube is difficult to pack so a good option is the hexagonal shape tube. They find also that a thinner adsorbent layer adsorbs moisture more efficiently and that porosity and tortuosity influence the moisture removal capacity.

Another solution is an air to water heat exchanger. This technology works in two separate phase: adsorption and regeneration. The shape of the exchanger is typical of finned batteries, with an internal pipe where the water flows. There are two choices to equip the battery with the adsorption materials; the first is to fill the space between fins with for example silica gel grains. While the second is to coat the fins surface with a thick layer.

The former is cheaper and technologically less complex but can have a critical problem due to the gravity force. In fact when the battery filled with silica gel grains stays for many time in a vertical position and it is not built perfectly, grains tend to bank on the lower part of the battery. The latter instead must be a thin layer for maximize the adsorption and for this reason it is very delicate because the layer can break and crack. When silica gel grains are used the mass quantity is bigger than the thin layer of zeolite; for this systems that use silica gel grains have more autonomy and the functioning is more stable.

3 ENERGY AND EXERGY ANALYSIS

In this paragraph is given the model of the system studied from an energy and exergy point of view. In particular the treatment is focused on the zeolite (SAPO-34) battery described on cap.3.2.1. This is done for the complete study of adsorption process and for the subsequent analysis of data. The equations used are obtained from elaboration and demonstration in accordance with the literature. The most important work examined is “*Advanced Engineering Thermodynamics*” of A.Bejan.

3.1 Energy analysis

This is the way to understand the mass and energy flux direction and this is the starting point for the subsequent exergy analysis. Primarily is good to define a control volume. This will be our domain where we will do the system energy balance. We considered the adsorption/regeneration system as only one control volume (Figure 20):

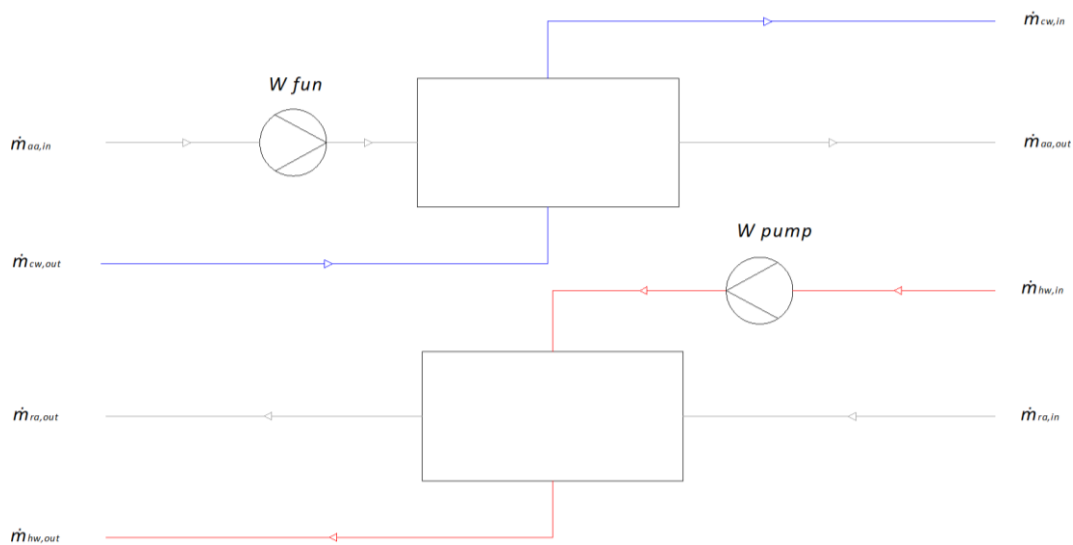


Figure 20 – Scheme of adsorption/desorption system control volume

We applied the first thermodynamic principle:

$$Q - \mathcal{L} = \Delta E \quad (27)$$

Where in our case:

$$\Delta E = \Delta U \quad (28)$$

Than for an open system:

$$\dot{Q} - \dot{L} = \sum_{out} \dot{m}_j h_j - \sum_{in} \dot{m}_j h_j \quad (29)$$

This is the energy balance with powers. Our study is done in a transitory so an energy balance is more appropriate:

$$Q - L = \sum_{out} \int_{t-1}^t \dot{m}_j h_j - \sum_{in} \int_{t-1}^t \dot{m}_j h_j \quad (30)$$

The enthalpy of a humid air stream is composed by two contributes. The first is a sensible contribute due to the temperature of the stream. The second is a latent contribute due to the humidity of the stream. The equation used is the following [18]:

$$h = h_a + x h_v \quad (31)$$

With:

$$h_a = c_{pa}(T - T_0) \quad (32)$$

$$h_v = r_0 + c_{pv}(T - T_0) \quad (33)$$

$$x = 0.622 \frac{\varphi P_s}{P - \varphi P_s} \quad (34)$$

$$P_s = \exp\left(a_1 \frac{t}{a_2 + t} + a_3\right) \quad (35)$$

With:

a1	a2	a3
17,438	239,78	6,4147

Table 1 – Parameters for saturation pressure experimental curves

Substituting equation (32) and (33) in (31):

$$h = c_{pa}(T - T_0) + x[r_0 + c_{pv}(T - T_0)] \quad (36)$$

Putting numerical values and express temperature in Celsius:

$$h = 1.006t + x(2501 + 1.875t) \quad (37)$$

It is evaluated, as energy parameters to compare, the coefficient of performance (COP) of the adsorption system. In [19] is show this expression as the ratio between the cooling power and the regeneration power. In our case is more convenient to give an energy expression:

$$COP = \frac{Q_{cool}}{Q_{reg}} = \frac{h_{ads,out} - h_{ads,in}}{h_{reg,in} - h_0} \quad (38)$$

3.2 Exergy analysis

Exergy analysis is a fundamental instrument to evaluate the efficiency of a process and then to make optimizations to increase its performances. With this technique is possible to determinate where inefficiencies are located. In fact it is possible to do an exergy analysis both on the single component and on the whole system. With a component as a control volume it is possible to establish what are the most inefficient components and so where the optimization is more relevant. Using the whole system as control volume it is possible to compare the system studied with another different system utilized for the same scope, such as conventional vapour compression system. In this analysis both studies are done. In the first study two different adsorption materials are compared on the same component. Then the whole system is compared with a heat pump working under the same condition.

3.2.1 Equations

The equation used is the classical exergy equation:

$$\dot{W} = \dot{m}(ex_1 - ex_2) - T_0\dot{S}_{gen} \quad (39)$$

The equation, like others works (e.g. [20]), uses the conservation of mass and energy principles with the second law. The exergy destruction ($T_0\dot{S}_{gen}$) includes the heat and mass transfer exergy destruction inside the zeolite battery ($T_0\dot{S}_{gen,tr}$) and the air mixing exergy destruction ($T_0\dot{S}_{gen,mix}$) at the outlet of the battery for both regeneration and processed air. So the exergy destruction is composed by exergy destruction of sensible heat transfer and exergy destruction of moisture transfer [21]. When the exergy analysis is done a dead state must be defined. This state is on equilibrium with the environment and at any energy at the same conditions is associated an exergy destruction flux. For humid air the exergy flux is composed by two different contributes, the physical and the chemical exergy. The first account mechanical and thermal works that the system can do respect to the dead state and the second the chemical work.

$$\bar{e}_t(T, P, x_i) = \bar{e}_{ph}(T, P) + \bar{e}_{ch}(T, P, x_i) \quad (40)$$

$$\bar{e}_{ph}(T, P) = \bar{h}(T, P) - \bar{h}^*(T_0, P_0) - T_0[\bar{s}(T, P) - \bar{s}^*(T_0, P_0)] \quad (41)$$

$$\bar{e}_{ch}(T_0, P_0, x_i) = \sum_{i=1}^n [\mu_i^*(T_0, P_0, x_i) - \mu_{0,i}(T_0, P_0, x_i)]x_i \quad (42)$$

The classical way of describing the thermodynamic properties of humid air is to treat it as an ideal gas mixture of two components (a, v) that individually exhibit ideal gas behaviour [22]. For example for air:

$$\bar{h}_a - \bar{h}_a^* = \bar{h}_a(T) - \bar{h}_a^*(T_0) = \bar{c}_{p,a}(T - T_0) \quad (43)$$

$$\bar{s}_a - \bar{s}_a^* = \bar{s}_a(T, P) - \bar{s}_a^*(T_0, P_0) = \bar{c}_{p,a} \ln\left(\frac{T}{T_0}\right) - \bar{R} \ln\left(\frac{P}{P_0}\right) \quad (44)$$

$$\mu_a^* - \mu_{0,a} = \mu_a^*(T_0, P_0, x_a) - \mu_{0,a}(T_0, P_0, x_{0,a}) = \bar{R}T_0 \ln\left(\frac{x_a}{x_{0,a}}\right) \quad (45)$$

The same evaluation can be done for the water vapour. So putting the equations together it is possible to write:

$$\begin{aligned} \bar{e}_t = & (x_a \bar{c}_{p,a} + x_v \bar{c}_{p,v})T_0 \left(\frac{T}{T_0} - 1 - \ln\left(\frac{T}{T_0}\right) \right) + \bar{R}T_0 \ln\left(\frac{P}{P_0}\right) \\ & + \bar{R}T_0 \left(x_a \ln\left(\frac{x_a}{x_{0,a}}\right) + x_v \ln\left(\frac{x_v}{x_{0,v}}\right) \right) \end{aligned} \quad (46)$$

Reporting the total flow exergy per kilogram of dry air and introduction the following parameters, the general equation become:

$$\omega = \frac{m_v}{m_a} \quad (46)$$

$$\tilde{\omega} = \frac{x_v}{x_a} \quad (47)$$

$$\tilde{\omega} = \frac{m_v/M_v}{m_a/M_a} = \frac{28.97}{18.015} \omega = 1.608\omega \quad (48)$$

$$\begin{aligned} e_t = & (c_{p,a} + \omega c_{p,v})T_0 \left(\frac{T}{T_0} - 1 - \ln\frac{T}{T_0} \right) + R_a T_0 \ln\frac{P}{P_0} \\ & + R_a T_0 \left[(1 + \tilde{\omega}) \ln\frac{1 + \tilde{\omega}_0}{1 + \tilde{\omega}} + \tilde{\omega} \ln\frac{\tilde{\omega}}{\tilde{\omega}_0} \right] \end{aligned} \quad (49)$$

For the exergy analysis the two phases are taken separately and taken into account together only in the efficiency equation. Exergy graphs show the parabolic trend that go to zero on the death state:

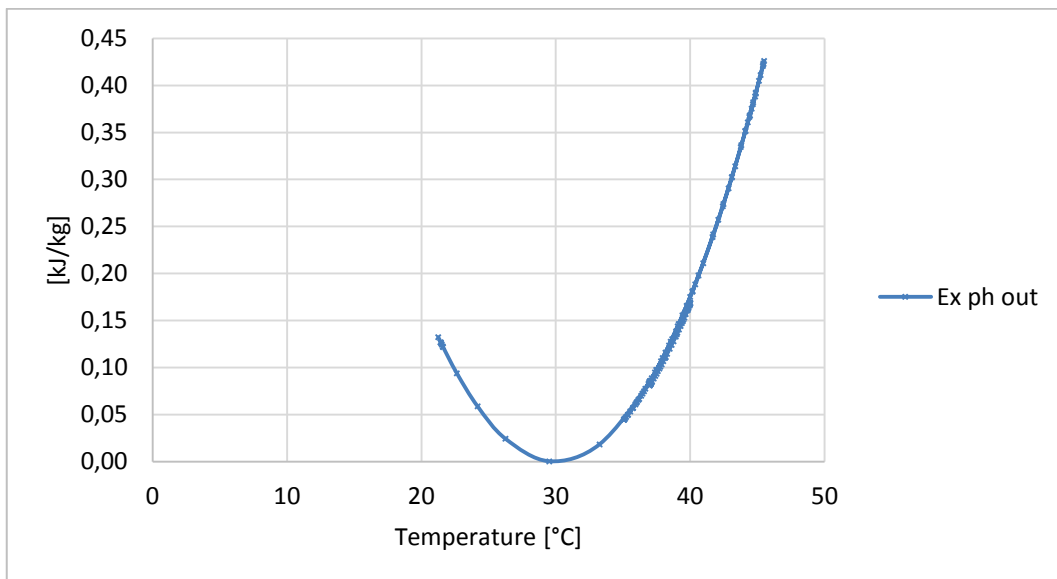


Figure 21 – Physical exergy in function of temperature

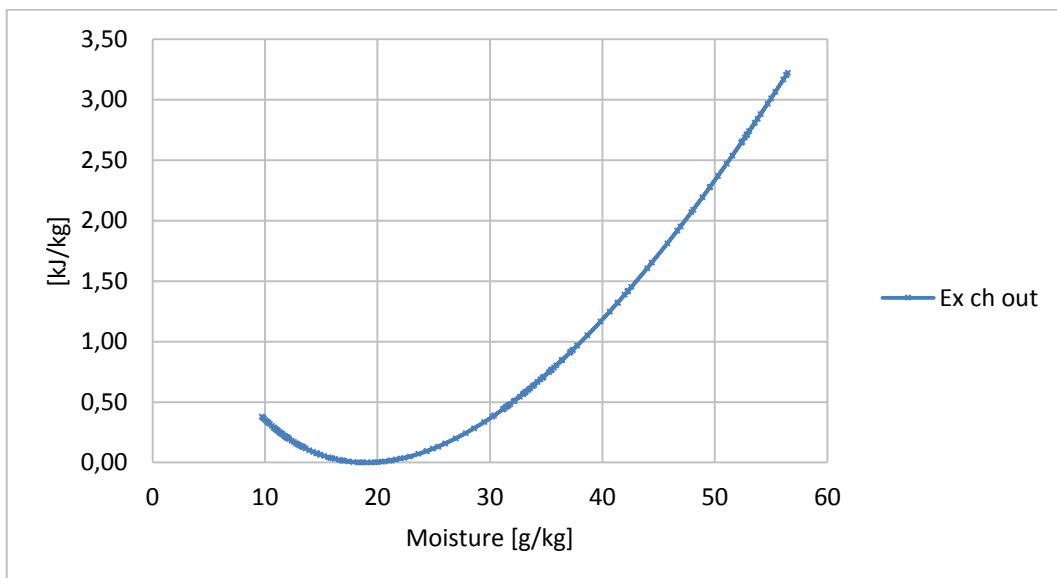


Figure 22 – Chemical exergy in function of moisture quantity

The dead state is assumed at least as the inlet condition (ambient condition). So it is:

T [°C]	x [g/kg]
30	19

Table 2 – Dead state

Exergy variation is the sum of physical and chemical contribution; first term is influenced by temperature while second by water vapour content. It is done a study about the variation of this parameter.

T (°C)	x 1	x 2	x 3	x 4	x 5	x 6	x 7	x 8	x sat
25	0,01	0,011	0,012	0,014	0,015	0,016	0,017	0,019	0,020
26	0,01	0,011	0,013	0,014	0,016	0,017	0,018	0,020	0,021
27	0,01	0,012	0,013	0,015	0,016	0,018	0,019	0,021	0,022
28	0,01	0,012	0,013	0,015	0,017	0,019	0,020	0,022	0,024
29	0,01	0,012	0,014	0,016	0,018	0,019	0,021	0,023	0,025
30	0,01	0,012	0,014	0,016	0,018	0,020	0,023	0,025	0,027
31	0,01	0,012	0,015	0,017	0,019	0,021	0,024	0,026	0,028
32	0,01	0,012	0,015	0,017	0,020	0,022	0,025	0,027	0,030
33	0,01	0,013	0,015	0,018	0,021	0,024	0,026	0,029	0,032
34	0,01	0,013	0,016	0,019	0,022	0,025	0,028	0,031	0,033
35	0,01	0,013	0,016	0,020	0,023	0,026	0,029	0,032	0,035
36	0,01	0,013	0,017	0,020	0,024	0,027	0,031	0,034	0,037
37	0,01	0,014	0,017	0,021	0,025	0,028	0,032	0,036	0,039
38	0,01	0,014	0,018	0,022	0,026	0,030	0,034	0,038	0,042
39	0,01	0,014	0,019	0,023	0,027	0,031	0,036	0,040	0,044
40	0,01	0,015	0,019	0,024	0,028	0,033	0,037	0,042	0,046

Table 3 – Parameters of humidity used for the study in table 4

In Table 3 – Parame is possible to see data used for the study. For all temperature has been chosen a interval between $x = 0,01 \text{ kg/kg}$ and $x = x_{sat}$ subdivided in nine values. Then specific exergy has been evaluated for each temperature and humidity values.

Specific exergy [kJ/kg]									
T (°C)	x 1	x 2	x 3	x 4	x 5	x 6	x 7	x 8	x sat
25	0,396	0,297	0,217	0,154	0,107	0,073	0,052	0,044	0,046
26	0,381	0,271	0,185	0,119	0,073	0,043	0,029	0,030	0,043
27	0,369	0,248	0,156	0,089	0,045	0,021	0,016	0,028	0,055
28	0,360	0,228	0,131	0,064	0,024	0,007	0,013	0,038	0,082
29	0,355	0,211	0,109	0,043	0,009	0,003	0,021	0,063	0,126
30	0,353	0,198	0,092	0,028	0,002	0,007	0,042	0,102	0,187
31	0,355	0,188	0,079	0,019	0,002	0,022	0,075	0,157	0,267
32	0,360	0,180	0,070	0,016	0,010	0,047	0,121	0,229	0,367
33	0,368	0,177	0,065	0,018	0,027	0,083	0,182	0,318	0,489
34	0,380	0,176	0,065	0,027	0,053	0,132	0,259	0,427	0,633
35	0,395	0,179	0,069	0,043	0,088	0,194	0,351	0,556	0,802
36	0,413	0,185	0,078	0,067	0,134	0,269	0,462	0,706	0,996
37	0,435	0,195	0,093	0,098	0,191	0,359	0,591	0,880	1,219
38	0,460	0,208	0,112	0,137	0,260	0,464	0,740	1,077	1,470
39	0,488	0,224	0,137	0,185	0,340	0,586	0,910	1,301	1,752
40	0,519	0,244	0,168	0,242	0,434	0,726	1,102	1,552	2,067

Table 4 – Data for Fig.23

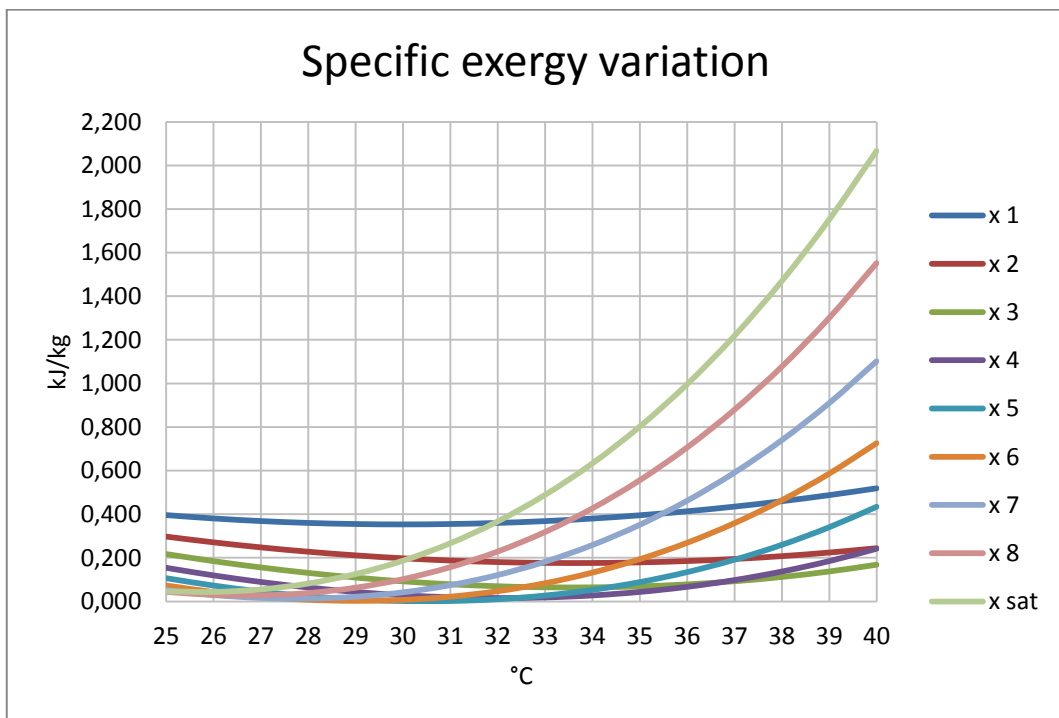


Figure 23 – Specific exergy variation with the temperature

It is possible to see how the two contribution together influenced the exergy trend. For example for low values of absolute humidity the curves never go to zero; this is characteristic for a parabolic trend with an exponential growing on the right and on the left of the death state. The death state is always the same.

The evaluation of exergy is done step by step for all time-steps. At the end a summation is done and the powers are transformed in energies.

Then the data accounted are elaborated to give the researched results.

3.2.2 Performance parameters

After energy and exergy analysis the way to put together all result is to evaluate some performance parameters. In [23] are identified both energy and exergy efficiency parameters. In the following section the equations are showed. The first parameter used is moisture removal capacity (MRC):

$$MRC = \dot{m}_p (\omega_{a,in} - \omega_{a,out}) \quad (50)$$

This parameter gives the uptake velocity of the air stream during adsorption phase. Instead from an exergy point of view the second-law efficiency is used. It is defined as the ratio between the exergy obtain by the process and the exergy in input:

$$\eta_{II} = \frac{Ex_{obt}}{Ex_{in}} \quad (51)$$

$$\eta_{II} = 1 - \frac{Ex_{loss}}{Ex_{in}} \quad (52)$$

We considered the whole process (adsorption and regeneration). So the efficiency is:

$$\eta_{II} = \frac{\sum_0^n \dot{m}_{ads} (e_{ads,in} - e_{ads,out}) \cdot \Delta t}{\sum_0^n (\dot{W}_{pump} \cdot \Delta t) + \sum_0^n (\dot{W}_{fun} \cdot \Delta t) + \sum_0^n (\dot{m}_{reg} (e_{reg,in} - e_{reg,out}) \cdot \Delta t)} \quad (53)$$

This ratio gives us the exergy efficiency of the process. The two batteries have a deeply different shape due to the two adsorbent materials. Silica gel battery is completely filled with many layer of grains (Figure 33 – Particular of the adsorbent material. On the left silica gel while on the right zeolite). This

characteristic leads to have higher pressure drops than the coated Zeolite battery. Is not possible to take into account directly for the heat flux needed for the regeneration because the average temperature between the cooling fluid and the battery is not known a priori. So the equation take into account of this heat flux directly with the exergy different between inlet and outlet air during regeneration.

3.3 Exergy comparison with an heat pump

For the comparison of the system with an heat pump working under the same conditions a different types of analysis is done (Figure 24). The first hypothesis done is the stationarity of the system. In fact the exergy analysis of the heat pump is done counting power streams (kW).

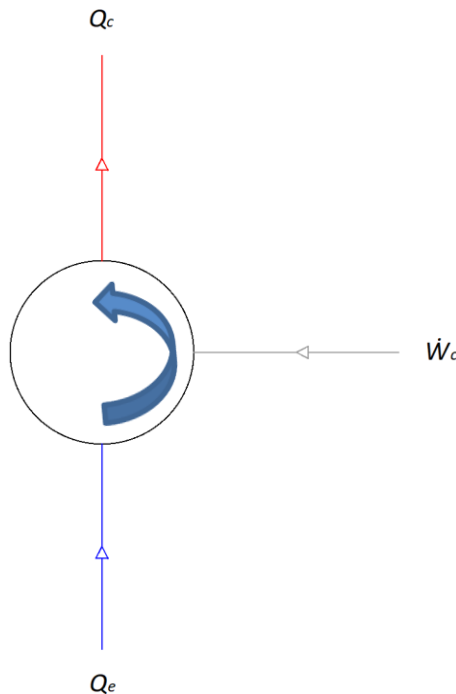


Figure 24 – Scheme of a heat pump

Performance parameters used in this section are three. Under an energy point of view the parameter is the COP_{el} (Coefficient Of Performance):

$$COP_{el} = \frac{|Q_H|}{W_{el}} \quad (54)$$

For the exergy analysis the parameter used is the second law efficiency. For the heat pump the equation is:

$$\eta_{II} = \frac{\dot{Q}_e \left(1 - \frac{T_0}{T_e}\right)}{\dot{W}} \quad (55)$$

Where \dot{Q}_e is the power needed for the same air processing of the adsorbent system while T_e is the average temperature inside the evaporator (equal to the temperature condensation of water vapour in that condition).

For the adsorbent system is:

$$\eta_{II} = \frac{\sum_0^n \dot{m}_{ads} (e_{ads,in} - e_{ads,out}) \cdot \Delta t}{\sum_0^n (\dot{W}_{pump} \cdot \Delta t) + \sum_0^n (\dot{W}_{fun} \cdot \Delta t) + \sum_0^n (\dot{m}_{reg} (e_{reg,in} - e_{reg,out}) \cdot \Delta t)} \quad (56)$$

This is the same equation of the previous evaluation.

4 EXPERIMENTAL TEST OF THE SYSTEM

4.1 *Test-Rig Description*

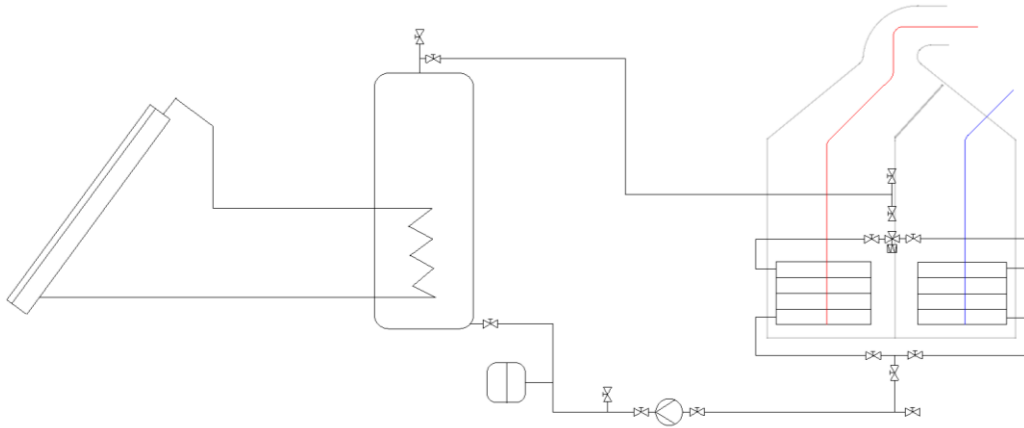


Figure 25 – System general scheme

The system is located in the laboratory of the department of energy, Galileo Ferraris, at the Politecnico di Torino (Figure 25). The system is composed by two water cycles and two air cycles. The outdoor components consist in 10 m² of vacuum tubes solar collectors on the roof of the department (Figure 26).

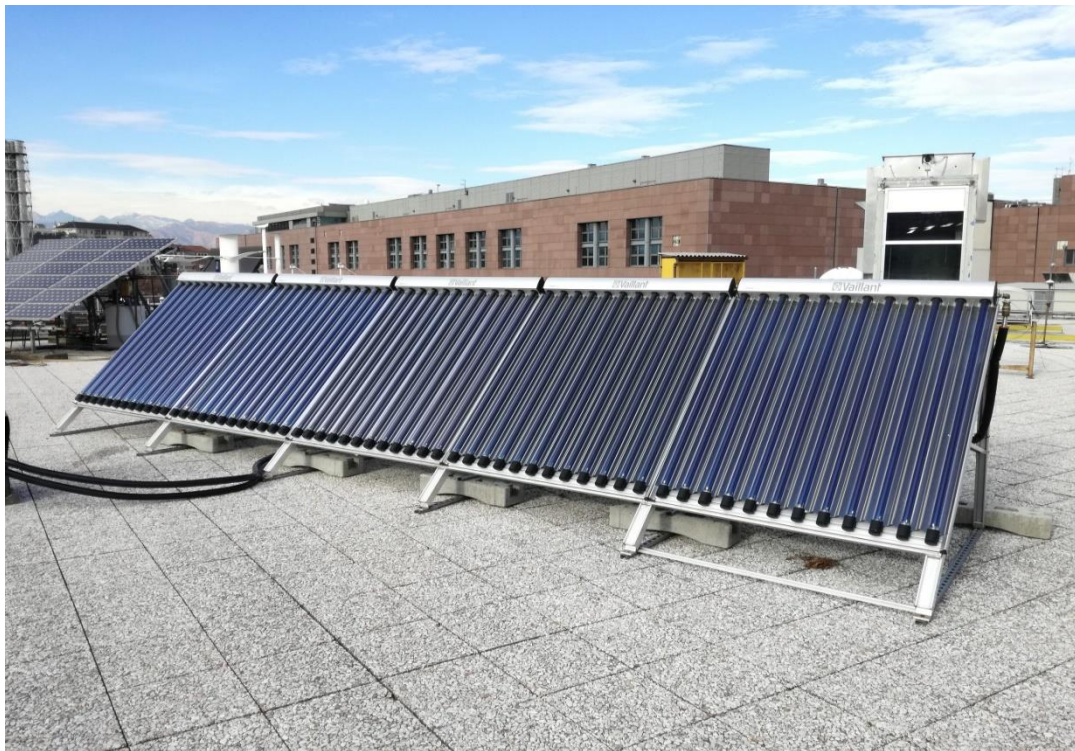


Figure 26 – Solar collectors on the roof of the laboratory

Solar collectors are linked with a heat storage in the laboratory that has a capacity of about 500 l and it is insulated with rigid polyurethane foam. The maximum working temperature is 90°C. It is composed by two water loops: the water loop connected with the solar collector and water loop connected with the system. Hot water of the secondary loop is used to regenerate the battery and it exchanges heat with the primary loop into the water tank. It goes into the adsorption module where a valve alternates the circulation in the two batteries. While a battery adsorbs water from an air stream other battery is crossed by the hot water desorbing humidity takes off by another air stream (Figure 27 – Adsorption and regeneration process on the battery).

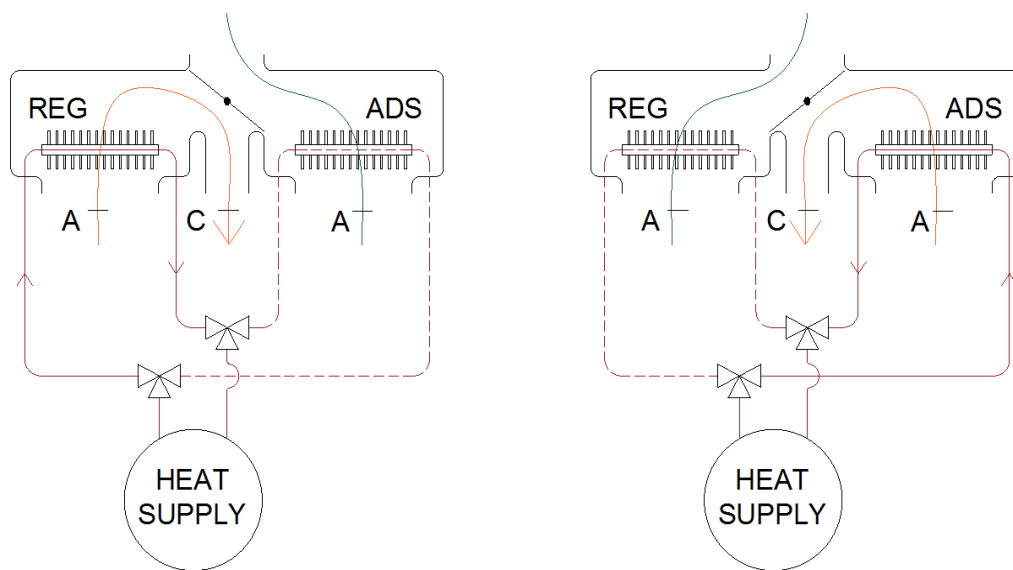


Figure 27 – Adsorption and regeneration process on the battery

On the return pipe a circulation pump is present. It has three levels of power (6 to 44 W) with a maximum water flow of 3 m³/h. After the pump an expansion vessel is present; this element permits the water to expand during the cycle. After the expansion vessel water return back into the heat storage (Figure 28).



Figure 28 – Water tank and water pump of the secondary loop

On this cycle many valves are present. Starting from the outlet of thermal storage: an air valve that permits to the air to go out from the storage, a spherical valve, another air valve, an electrical control valve that permits to drive the water flux in one or other battery following by two manual spherical valves, three manual spherical valves on the outlet of batteries, an air valve, two manual spherical valves one before and one after the pump, an air valve and a valve before the inlet of thermal storage. In the desiccant system there is a dump that rotates and permits the alternation of the two air streams. The air flow inlet is in the low part of the structure; air is provided by an UTA (Unit Air Treatment) that guarantees a fixed temperature (Figure 29).



Figure 29 – UTA

The two batteries are equal; only the type of adsorber changes. In the following table are reported all dimensions:

	d [mm]	n	δ [mm]	p [mm]	L [m]	D [m]	H [m]	V [m ³]
Fins	-	90	0,2	5	-	0,13	0,54	0,00126
Tubes	15	24	-	-	0,45	-	-	0,00111
Battery	-	-	-	-	0,45	0,13	0,54	0,03159

Table 5 – Battery dimensions

The following figure shows a schematic structure of the batteries:

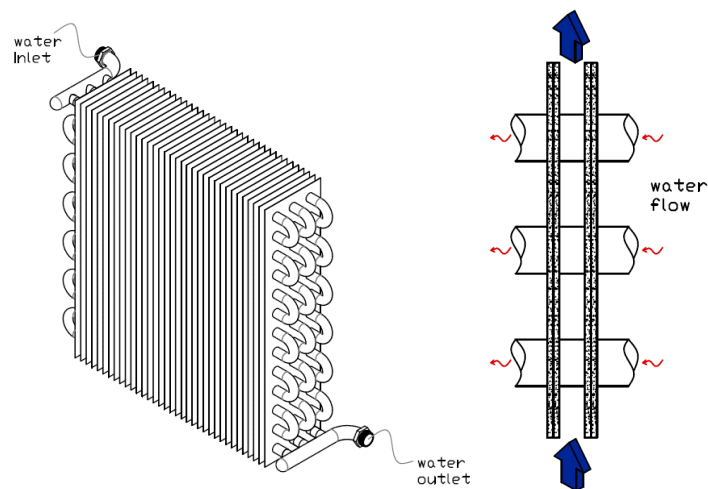


Figure 30 – Structure of the two batteries

Air crosses the battery and the water vapour is adsorbed. During this procedure is possible to provide to the battery cold water in order to promote the adsorption, with also a cooling effect on the air. Air then goes out from the desiccant system dried. During the regeneration the dump switches and the air flow is directed out through a shutter. A hot water flow coming from the heat storage crosses the battery to regenerate the adsorbent material. An ambient air flow drop out the removed humidity. In the system studied the two batteries present two different configurations. One is a finned tube heat exchanger filled with small grains of silica gel (Figure 31); the other is a finned heat exchanger coated with a thick layer of Zeolite (Figure 32) (Figure 33).



Figure 31 – Silica gel battery

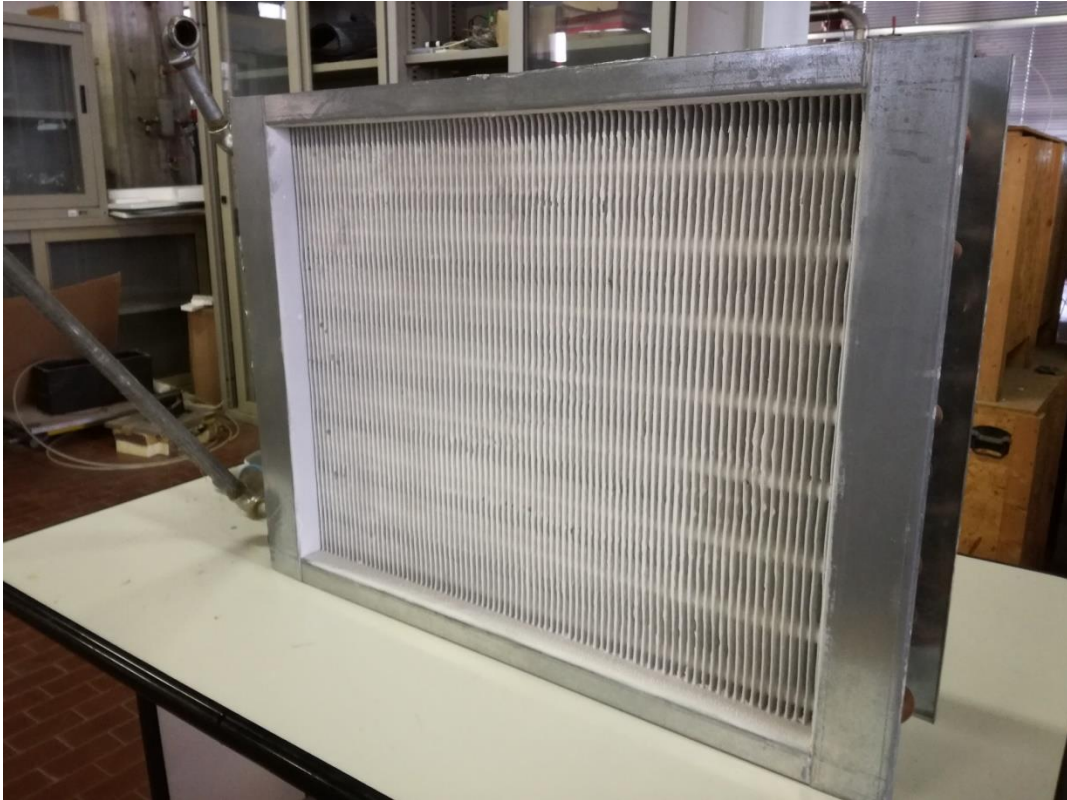


Figure 32 – Zeolite battery



Figure 33 – Particular of the adsorbent material. On the left silica gel while on the right zeolite

Both two can have some functional problems. Two of the most important are the banking of grains in the bottom of battery for silica gel and the cracking of the thin layer for zeolite. The first happens when the battery filled with silica gel grains stays for many time in a vertical position and it is not built perfectly, grains tend to bank on the lower part of the battery (Figure 34).



Figure 34 – Banking of silica gel grains

The second when the battery is subjected to vibrations and shocks (Figure 35).

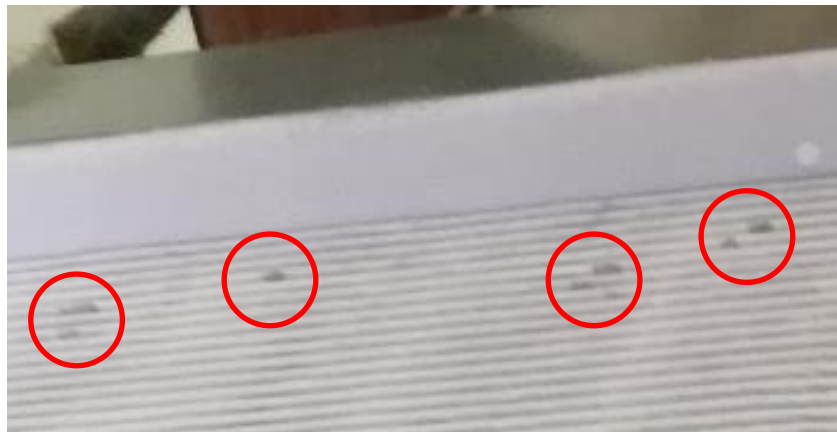


Figure 35 – Cracking of zeolite layer

The connection for the cooling system has been built appositely for these tests. It consist in a double connection, one for the supply water and one for the return, with electric valves. Two feelers are put near the two valves. These measurements give us the temperature of water in input and output the adsorption battery. They are put upside down because the feeler holder has to be dipped for the measurement detection (Figure 36).



Figure 36 – Cooling connections

The electric panel is sub-divided in three parts. The upper part consist in an automation interfaces composed by ten modules. These modules are essential for data acquisition and for setting and control of the system operation. The first module is a data-logger; it is the brain of the hole control system and its function is to linked all modules with a terminal like a computer. It collects data, analysing in real time and communicating them with other devices through Ethernet cable or wireless links. There are four modules for the analogue signals acquisition that can be expressed in potential or current terms in a certain rage (± 2.5 Vdc, ± 10 Vdc and ± 20 mA). Then two modules for digital signals are present; one for input signals and one for output signals. These modules are important for the control of mechanical parts, that can be handle directly on the lab-view. A module for the energy count is present and it is necessary for the correct acquisition of energy consumption. Then there are two modules for the data acquisition from NTC temperature sensors. These are characterized from three different conversional scales ($100 \Omega - 10 \text{ k}\Omega$, $1\text{k}\Omega - 100 \text{ k}\Omega$, $5 \text{ k}\Omega - 500 \text{ k}\Omega$). In the middle part

terminal blocks for the connection of modules with sensors are present while in the bottom part there is the generator and some relays.

In the following figure there is the electric panel project with the corresponding sensor on the system:

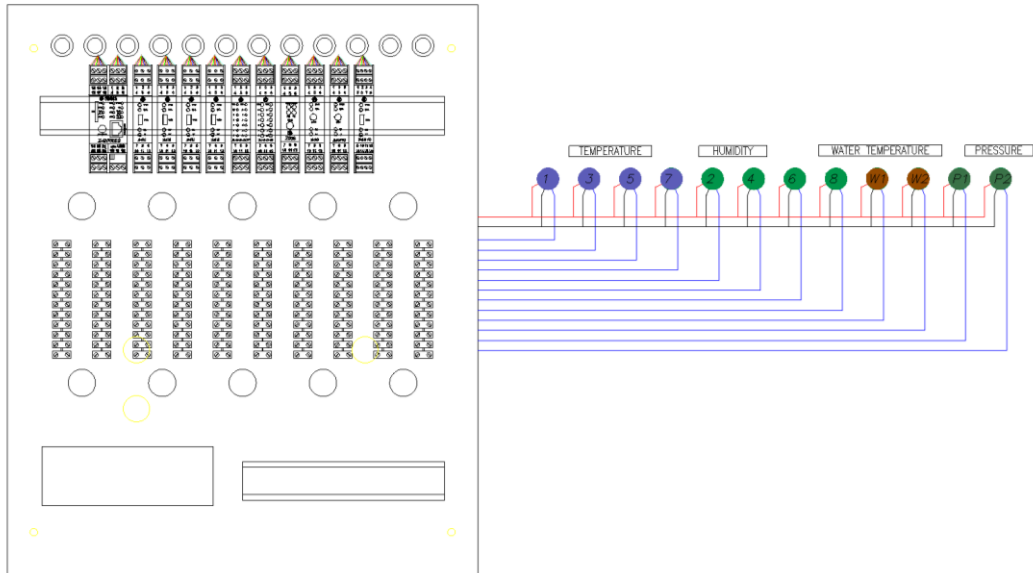


Figure 37 – Control panel scheme

In the following figure is given a sensor legend of the wall. Odd numbers and blue circles are for temperature sensor, while even numbers and green circles are for humidity sensors. Then there are cooling water and pressure drops sensors.

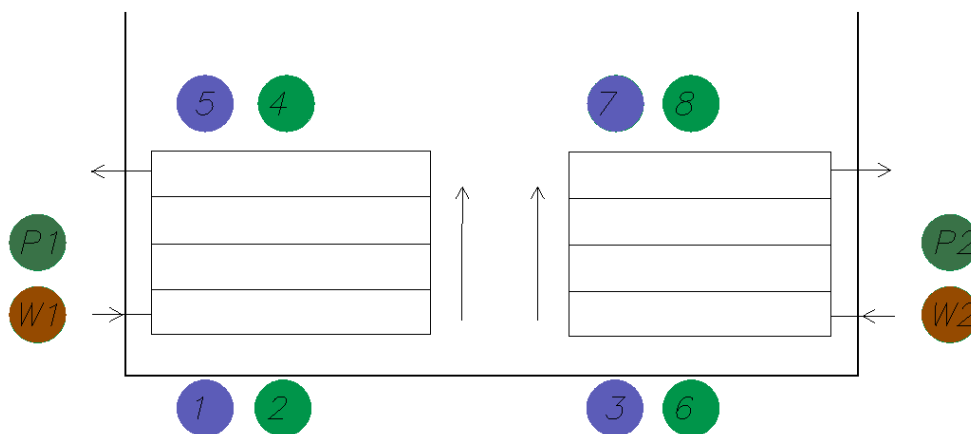


Figure 38 – Sensors scheme

This legend is used directly on the sensors located on the adsorption wall.

4.2 DAQ and sensor calibration

The target of the experiment is the calibration of sensors that acquires data from the system. The measurement requires a constant temperature bath. The feeler of the sensor is put into the bath and a multimeter measures the resistance between the clamps. The experiment is done for all sensor at four different temperature levels. Then a plot is done. These curves give us the relation between resistance and temperature.

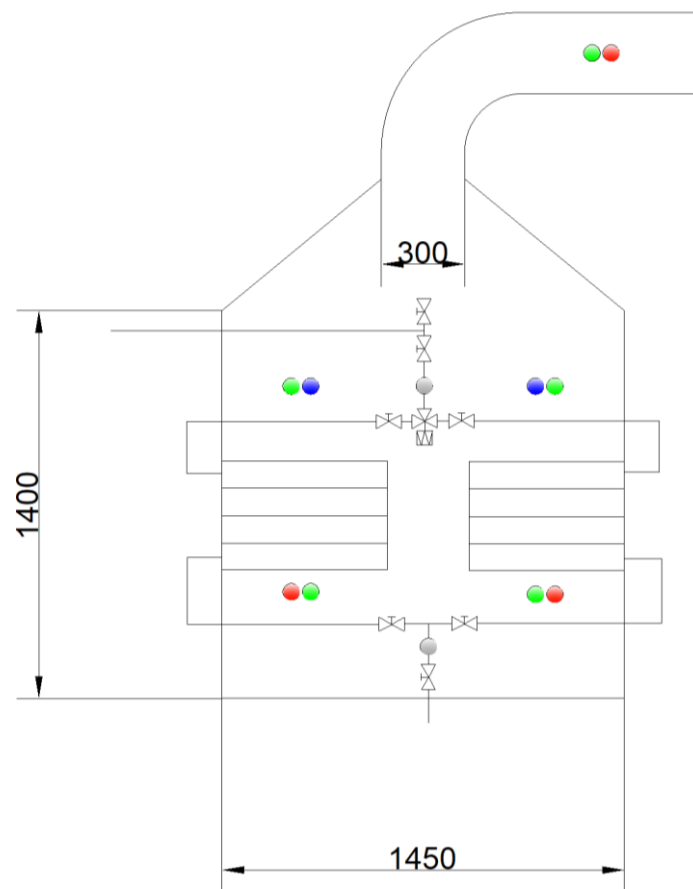


Figure 39 – Sensors position on the wall

- SHD100: humidity sensor
- STD100-300: temperature sensor in duct
- STP100-50: temperature sensor in pipe
- STD300-300: temperature sensors in duct

Others four sensors are on the back of the wall.

4.2.1 Objective

- Recalibration of air temperature sensor NTC1.8k of the NAC wall test rig
- Recalibration of the air temperature sensor Pt100 of the NAC wall test rig
- Plotting data
- Interpolation equation to be implemented in the data acquisition software

4.2.2 Method

There are nine temperature sensors on the NAC wall. Five of them have a sensor called Pt100. This sensor is made in Platinum and it has a resistance of 100 Ω at 0°C. The technology takes advantage of the accurate resistance/temperature relationship of the material. This relationship is translated in a linear equation:

$$R(T) = R_0 \cdot [1 + \alpha(T - T_0)] \quad (57)$$

Where:

$$R_0 = 100 \Omega \text{ (for Pt100)} \quad (58)$$

There is also a more accurate relation with a third order equation.

NTC means *Negative Temperature Coefficient*. These thermistors are made of a semiconductor material with a negative temperature coefficient; when the temperature increases the resistance decreases. NTC1.8k means that the resistances at 25°C is equal to 1.8 k Ω ($R_{25} = 1.8 \text{ k}\Omega$). For the sensors calibration a temperature constant bath is used; sensors are connected with a multimeter and then are put into the bath for two minutes (for the temperature equilibrium). For the NTC1.8k sensors measurements are done in Ohm (Ω), for the Pt100 sensors are done in Volt (V). The procedure is repeated for four different temperature levels: 0 °C, 20 °C for NTC1.8k and 25 °C for Pt100, 30 °C, 60 °C and 84 °C. Then curves are plotted and interpolation equations are extracted. At the end sensors are re-installed on the wall.

4.2.3 Results

Results are shown in the tables and figures below:

NTC1.8k Ω sensor:

STD100-300(sx)		STP100-50(sx)		STD100-300(dx)		STP100-50(dx)	
T (°C)	Ohm (Ω)	T (°C)	Ohm (Ω)	T (°C)	Ohm (Ω)	T (°C)	Ohm (Ω)
84,0	257	84,0	258	84,1	255	84,1	258
84,1	256	84,1	257	84,1	255	84,1	258
84,1	256	84,1	257	84,1	255	84,1	258
84,1	256	84,1	259	84,0	256	84,1	257
59,9	523	59,9	523	60,0	521	60,0	525
59,9	523	60,0	525	60,0	522	60,0	525
59,9	523	59,9	524	60,0	522	60,0	525
60,0	523	59,9	526	60,0	522	60,1	526
30	1462	30,0	1460	30,0	1460	30,0	1462
30	1462	30,0	1461	30,0	1461	30,0	1461
30	1462	30,0	1462	30,0	1460	30,0	1460
21,9	2000	21,7	2020	21,9	2000	21,7	2020
0	5080	0	5010	0	5090	0	4990

Table 6 – Experimental results of NTC sensors

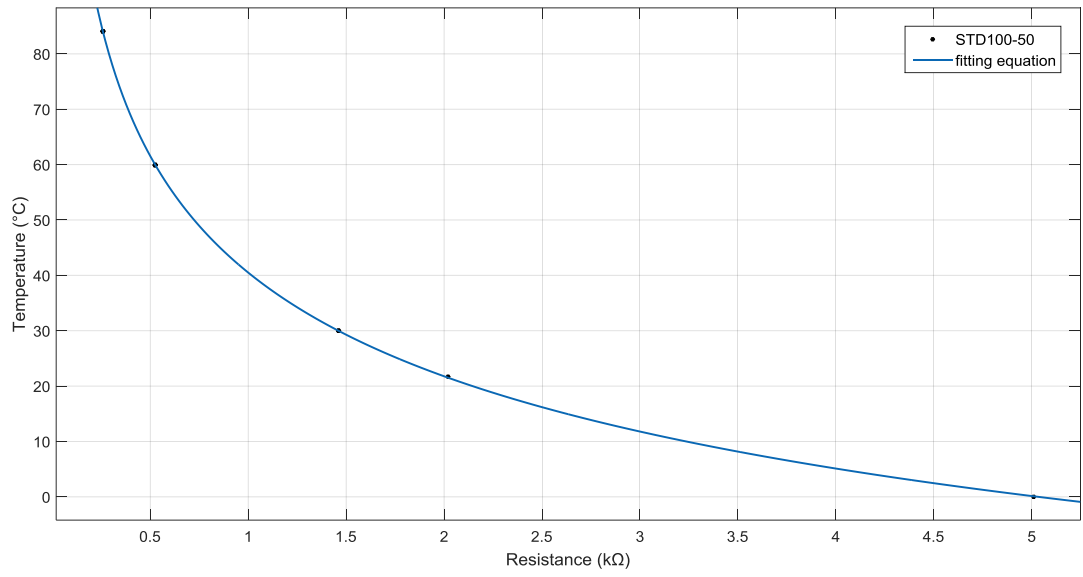


Figure 40 – STD 100-50 calibration curve

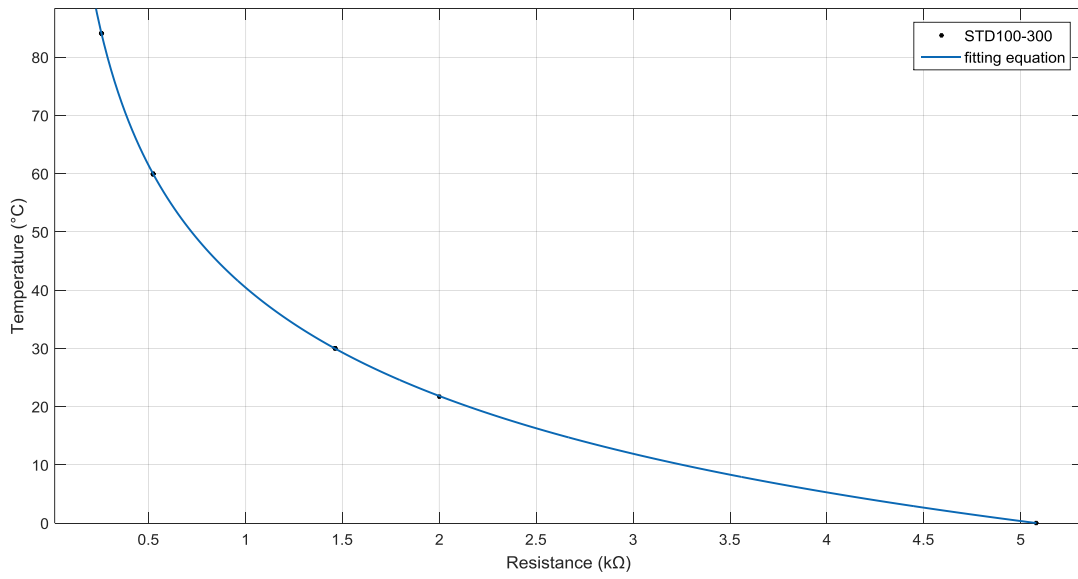


Figure 41 – STD 100-300 calibration curve

Pt100 sensors:

STD300-300 (b/sx)		STD300-300(b/dx)		STD300-300 (f/a)		STD300-300 (r/sx)		STD300-300 (r/dx)	
T (°C)	Tension (V)	T (°C)	Tension (V)	T (°C)	Tension (V)	T (°C)	Tension (V)	T (°C)	Tension (V)
0	0	0	0,01	0	0,01	0	0	0	0,01
25	2,53	25	2,55	25	2,52	25	2,54	25	2,55
30	3,04	30	3,05	30	3,02	30	3,04	30	3,05
60	6,04	60	6,05	60,1	6,03	60,1	6,06	60,1	6,05
84,1	8,45	84,1	8,47	84,1	8,43	84,1	8,47	84,1	8,46

Table 7 – Experimental results of Pt100

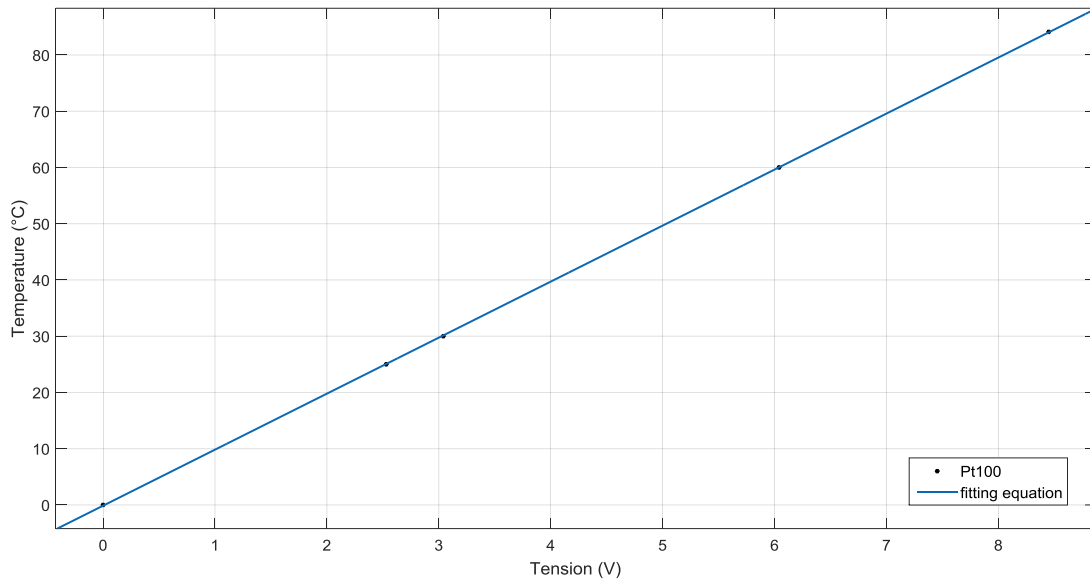


Figure 42 – Pt100 calibration curve

4.2.4 Final equations

From the previous analysis it is possible to take two interpolation equations, one for NTC sensors and one for Pt100, to use during the experiment. In fact all NTC equations and Pt100 equations are very similar among them. For NTC a fourth order equation is taken while for Pt100 a first order equation is taken.

For NTC sensors:

$$f(x) = ax^b + c \quad (59)$$

With for STD 100-50 (Figure 40):

a	b	c
170,3	-0,1679	-129,9

Table 8 – STD 100-50 curve parameters

And for STD 100-300 (Figure 41):

a	b	c
167,1	-0,1704	-126,7

Table 9 – STD 100-300 curve parameters

For Pt100 (Figure 42):

$$f(x) = p_1x + p_2 \quad (60)$$

With:

p1	p2
9,96	-0,137

Table 10 – Pt100 curve parameters

4.3 Tests

The experiment is done in the laboratory of the department of energy, Galileo Ferraris, at the Politecnico di Torino. The system is controlled by an interface on a computer (lab-view) linked with the electric control unit by an Ethernet cable. Before to start the experiment a sensors control is done. It is important to have an accurate maps of all sensor mounted on the system to take control of phenomena. The UTA provide an air flow with characteristics of humidity and temperature pre-established. The best situation would be have an ambient air stream already with the right characteristics because humidity and temperature would be more stable. Unfortunately the experiment is done in winter so an auxiliary humidifier is needed. The unit is equipped with an humidifier and an electric resistance to control humidity and temperature of the air stream. Before the adsorption test a regeneration is done. Therefore the battery is ready for the test. The adsorption phase is performed with a cooling water flow inside the battery and it ends when the humidity ratio in output is the same of the input. Immediately after, the regeneration phase starts. This phase is done in natural convection so the UTA does not provide any air flow. The experiment ends when the humidity ratio in output is the same of input. The regeneration is done with hot water provided by an electric resistance; in a normally working this hot water would be provided by solar collectors. The experiment is repeated with different air flow rates: Test-1 refers to an air flow of 220 m³/h, Test-2 refers to an air flow of 335 m³/h and Test-3 to an air flow of 430 m³/h. The first part of the curves is related to the adsorption process while the second to the regeneration. In the following table are reported all hypothesises for the three experiments:

		t [s]	Q [m ³ /h]	v [m/s]	T in [°C]	x in [g/kg]	ρ [kg/m ³]	h [kJ/kg]	ex in [kJ/kg]	T w [°C]
Test 1	Ads	1647	220	0,49	27	17,0	1,16	70,38	0,05	15
	Reg	1722	40	0,09	27	7,7	1,16	46,62	0,62	60
Test 2	Ads	1350	335	0,74	31	17,0	1,14	74,19	0,04	15
	Reg	1509	67	0,15	30	7,4	1,15	48,67	0,64	60
Test 3	Ads	891	430	0,95	30	15,3	1,15	69,29	0,07	15
	Reg	1329	80	0,18	30	6,7	1,15	46,78	0,74	60

Table 11 – Functional hypothesis

In the following graphs are reported the trend of air temperature and humidity in inlet and in outlet during the experiments.

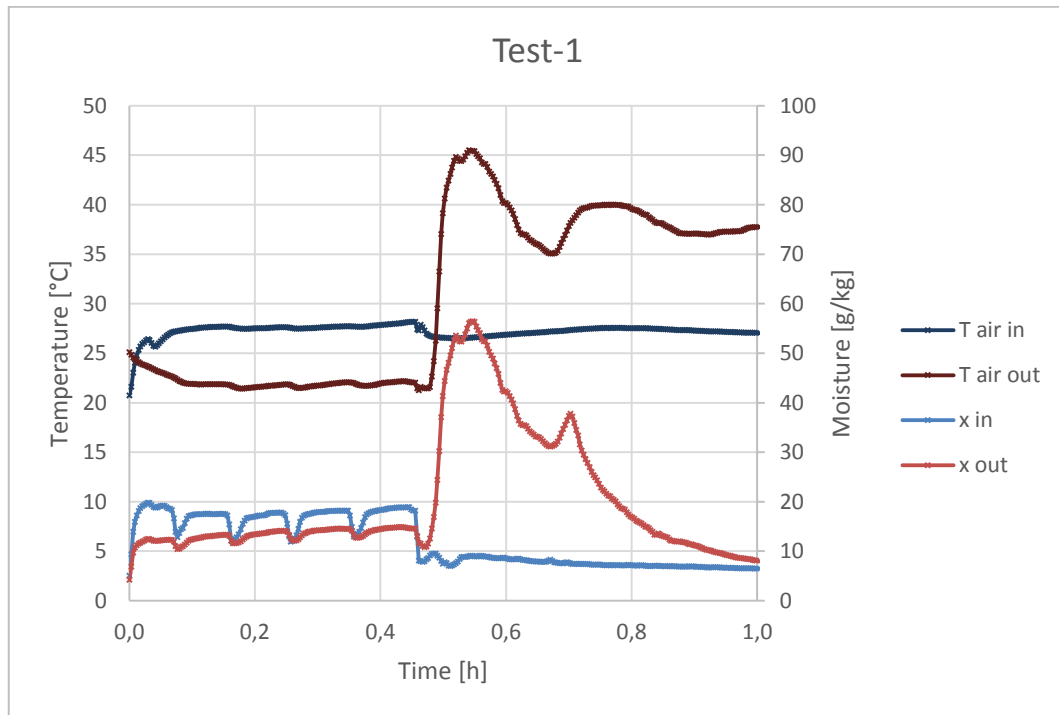


Figure 43 – Test-1: adsorption and regeneration with an air stream of 220 m³/h

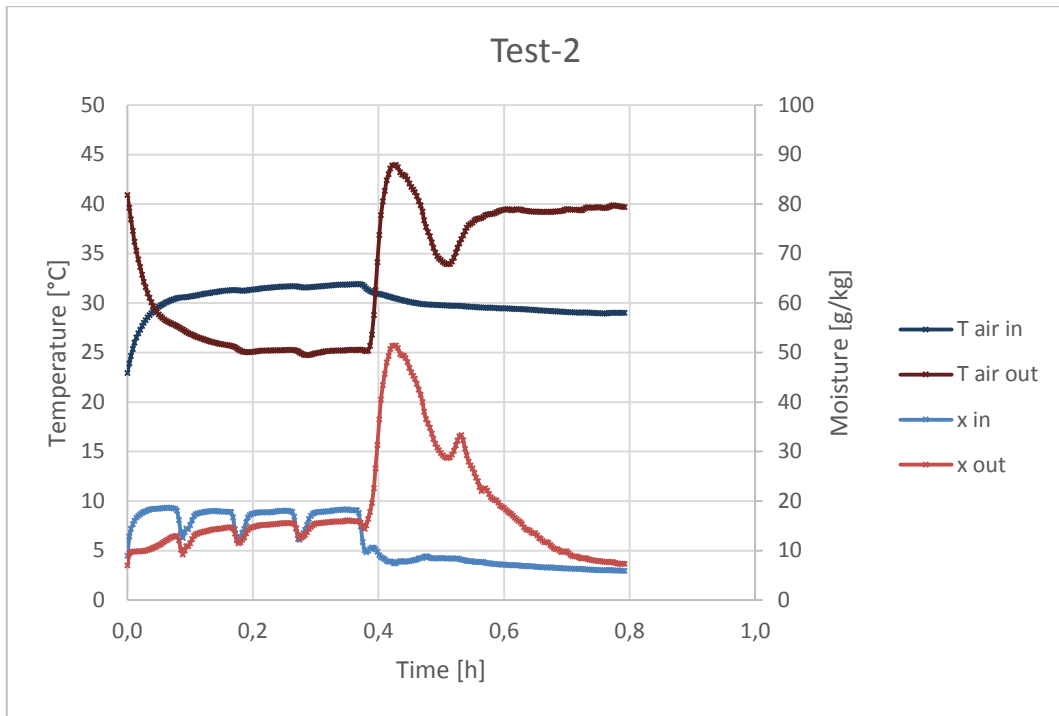


Figure 44 – Test-2: adsorption and regeneration with an air stream of 335 m³/h

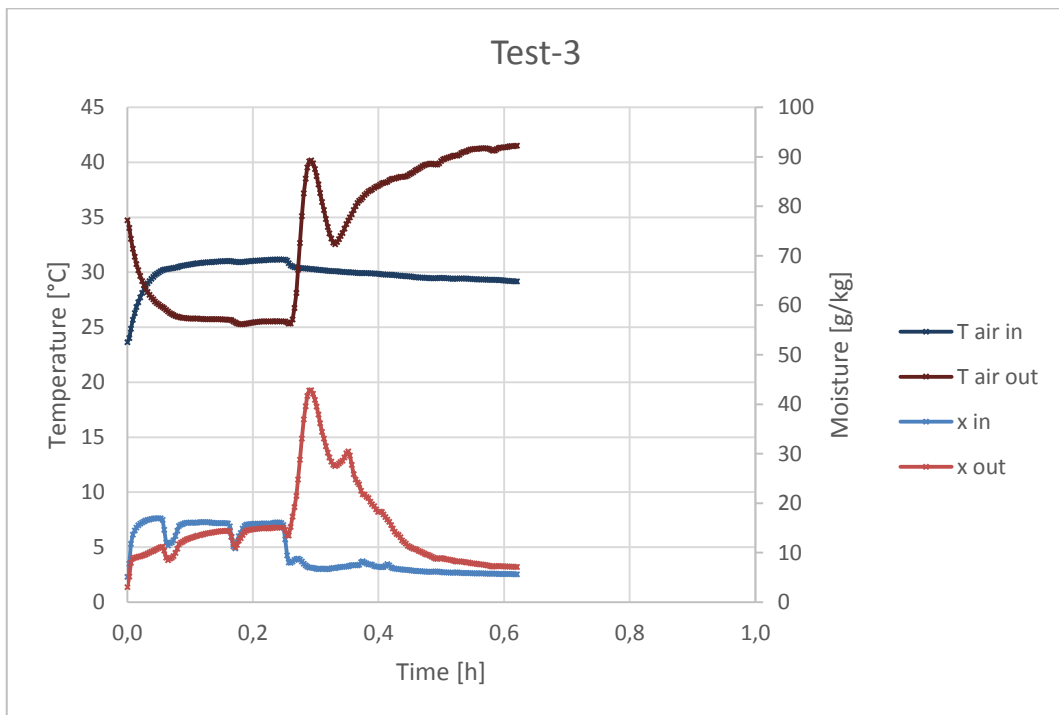


Figure 45 – Test-3: adsorption and regeneration with an air stream of 430 m³/h

It is possible to see that with a higher air flow rate the experiment duration is lower. The lower peaks of the humidity in inlet are due to a problem of UTA humidifier (see Table 20 – Time when the UTA humidifier shuts down). The high value of

absolute humidity during regeneration is due to the fact that this phase is done with natural convection conditions. It is possible to see that the duration time of experiment depend from the air flow rate. From the study is possible to see that for the first two flow rate the water uptake is quite the same while for the maximum flow the water uptake is lower. Regarding the air temperatures is possible to see that the cooling process, that improves the adsorption process, does a cooling effect also on the air stream. This means that in output the air does not need any process to reach the standard condition. On average the two phases have the same duration. It is also evaluated the heat power subtracted during adsorption and the heat power provided during regeneration (Figure 46).

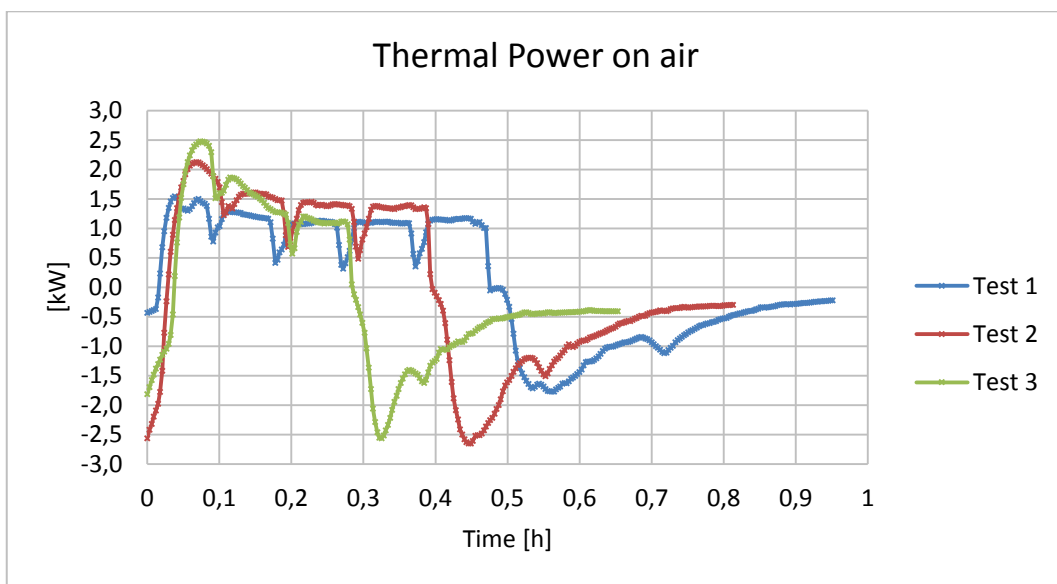


Figure 46 – Thermal power on air during adsorption/regeneration process

Evaluating the powers in function of time is possible to see that the two energies are very similar. This is highlighted by the evaluation of the thermic COP.

	Q ads [kJ]	Q reg [kJ]	COP th
Test 1	1778,07	1389,96	1,28
Test 2	1827,60	1513,74	1,21
Test 3	1343,28	1166,29	1,15

Table 12 – Heat flux exchanged

The electric consumption is very different between the two phases. In fact during adsorption only the fan works while during the regeneration only the pump. It is clear that the work on a liquid is a few order bigger than a work on an air stream (Figure 47).

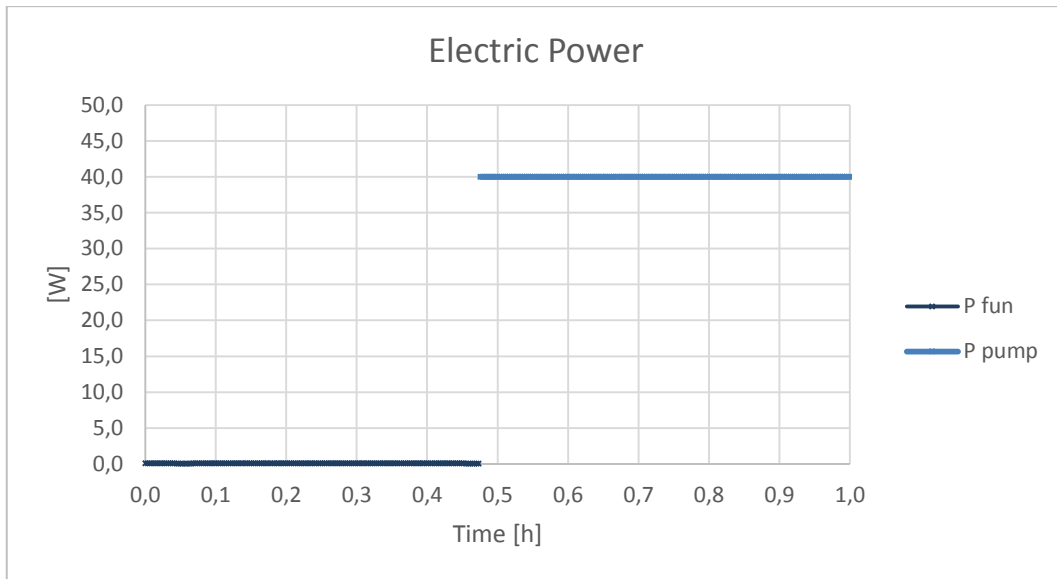


Figure 47 – Electric power consumption during the adsorption/regeneration experiment

The electric consumption due to the fun is negligible respect to the electric consumption due to the pump. Then the electric COP is evaluated:

	E el pump [kJ]	E el fun [kJ]	COP el
Test 1	68,88	0,10	25,78
Test 2	60,36	0,63	29,96
Test 3	53,16	1,40	24,62

Table 13 – Electric consumption

The laboratory availability has not permitted to perform the experiment on silica gel grains battery. So is not possible to give an exhaustive and appropriate comparison of the two technologies. But it is reported an old experiment performed under different conditions to give an idea of the phenomena behaviour (Figure 48).

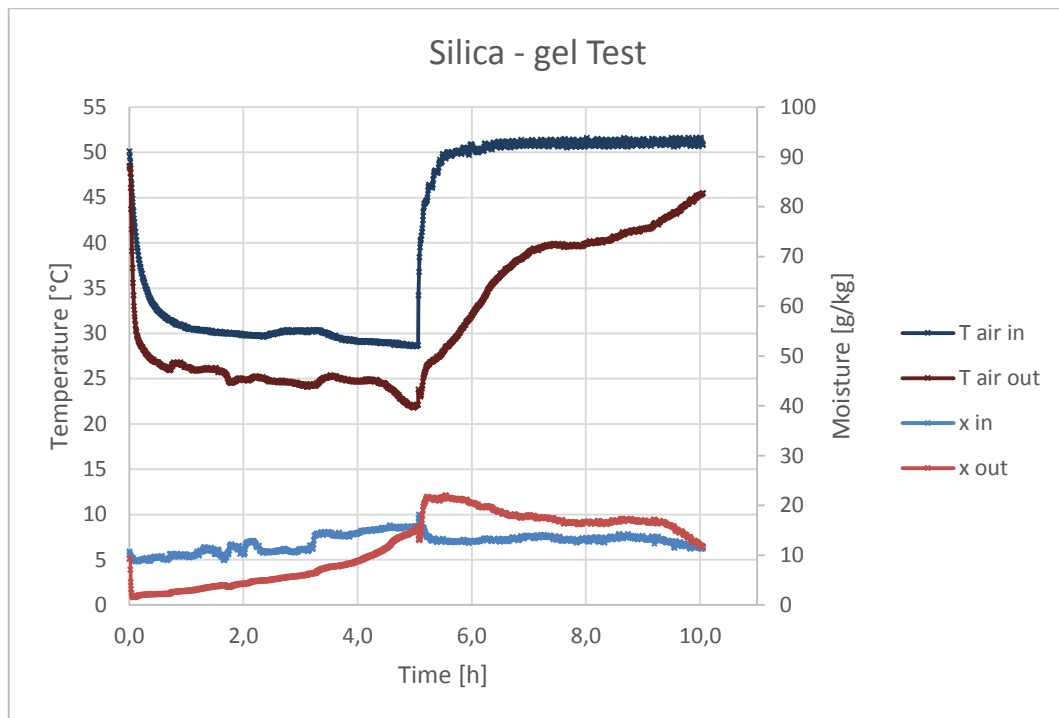


Figure 48 – Silica gel test (old experiment)

From the figure is possible to see the higher duration of the two phases with the silica gel grains packed bed. It is important highlight that the absolute humidity in input is lower than the zeolite experiments; so this behaviour leads to an increase of system adsorption autonomy. Despite this though the silica gel packed bed has an adsorption phase duration longer than zeolite coated layer. The main reason is the amount of adsorbent material; in a grains packed bed the mass of adsorber is higher than in a coated layer battery. This permit an higher amount of water subtracted. Is clear also that for the regeneration in this test has been used hot air and not hot water. The COP and the second law efficiency are deeply affected by these factor so the comparison cannot be appropriate. It would be interesting test this configuration with the hot water regeneration.

4.3.1 Pressure drops

As on others conditioning or dehumidification systems pressure drops are present. Pressure drops depends by many factors: rate of empty space, air velocity, crossing area, bed depth, air temperature etc. [6] and consequently is possible to act on these parameters to minimize pressure drops. The basics concepts for the evaluating and description of pressure drops in packed bad can be studied without considering the effect of confining wall [24]. It is important to have an high rate

of empty space to guarantee a good air crossing, air velocity must be not so high and the crossing area must be large and without obstacles. At the end a thick bed depth is preferred. The Kepler's conjecture says that in a packing of hard sphere is impossible to reach a porosity less than:

$$\varepsilon = 1 - \frac{\pi}{\frac{\sqrt{3}}{2}} \approx 25.95 \% \quad (61)$$

Concerning packed bed grains [6] says that with a random packing of hard spheres in three dimensions is possible to reach a density of 63.4%. In [25] are studied cubic and hexagonal packed beds on parallel walls structure; volume fraction depending on the ratio between distance of the walls and spheres diameter reaches values between 35% to 65% more or less.

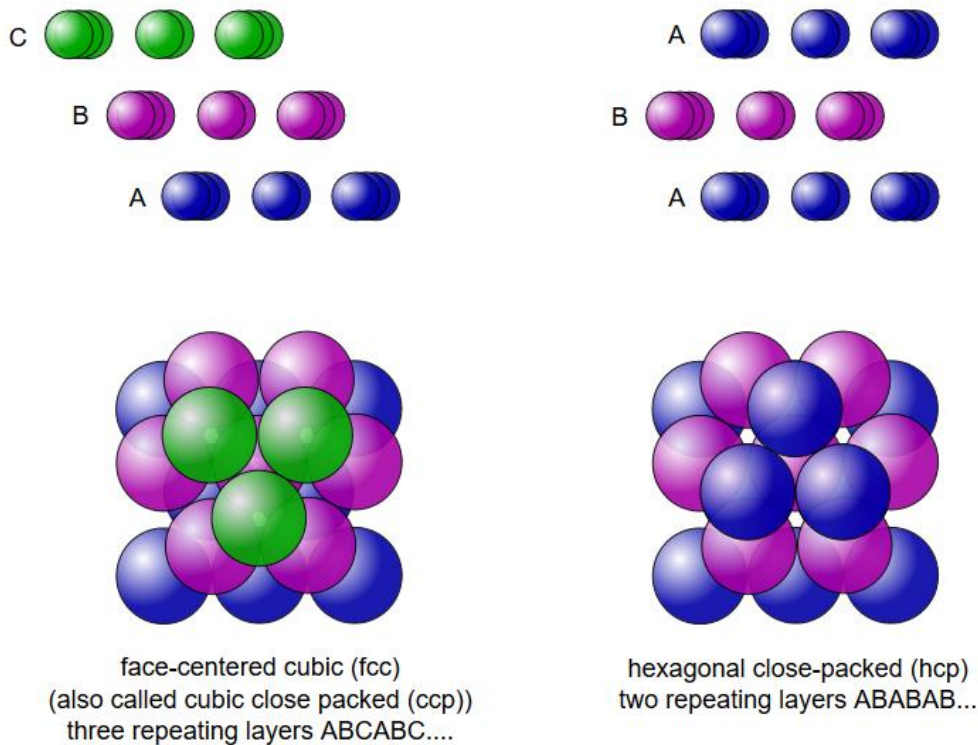


Figure 49 – Molecular structure of different package

For the analysis of pressure drops a random packaging is considered. A semi-empirical equation is used to relate the bed porosity with the ratio between the step of the fins and the particle diameters. This equation is exposed in [25]:

$$1 - \varepsilon = \frac{\pi}{3\gamma \frac{p}{d} \sqrt{3 - 4 \left(\frac{p}{d} - 1\right)^2}} \quad \text{for: } 1 \leq \frac{p}{d} \leq 1 + \sqrt{\frac{1}{2}} \quad (62)$$

$$1 - \varepsilon = \frac{2\pi \left(2 - \frac{p}{d}\right)}{3\gamma \sqrt{3 - 4 \left(\frac{p}{d} - 1\right)^2}} \quad \text{for: } 1 + \sqrt{\frac{1}{2}} \leq \frac{p}{d} \leq 1 + \sqrt{\frac{2}{3}} \quad (63)$$

$$1 - \varepsilon = \frac{2\pi}{3\gamma \frac{p}{d} \sqrt{3}} \quad \text{for: } 1 + \sqrt{\frac{2}{3}} \leq \frac{p}{d} \leq 2 \quad (64)$$

In the tables below are reported the input data for the study:

p (mm)	d (mm)			
	2,5	3	3,5	4
4	1,60	1,33	1,14	1,00
5	2,00	1,67	1,43	1,25
6	2,40	2,00	1,71	1,50
7	2,80	2,33	2,00	1,75
8	3,20	2,67	2,29	2,00
9	3,60	3,00	2,57	2,25

Table 14 – Dimension of fins

Results are shown in the following plot:

p/d	1-ε
1,000	0,568
1,143	0,504
1,250	0,475
1,333	0,462
1,429	0,458
1,500	0,464
1,600	0,492
1,667	0,534
1,714	0,574
1,750	0,568
1,810	0,610
2,000	0,568

Table 15 – Results

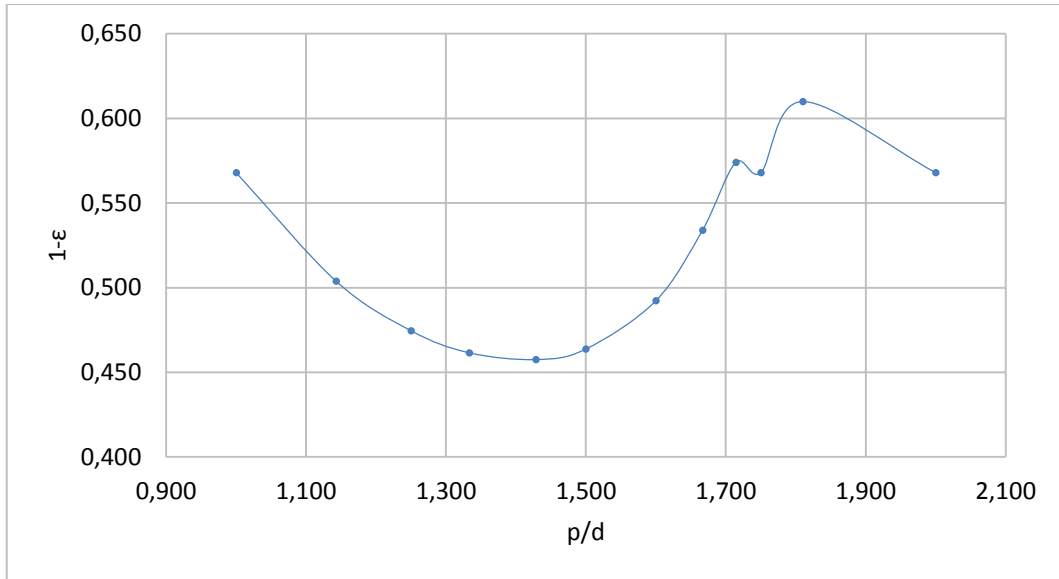


Figure 50 – The correlation between porosity and fins dimensions for the silica gel battery

The equation used to estimate theoretically pressure drops is the Ergun's equation [6]. This derived from Darcy relation. Air velocity is assumed to be constant and the silica gel grains as a spheres:

$$\Delta P_{ERGUN} = \left(150 \frac{(1 - \varepsilon)}{Re} + 1.75 \right) \left(\frac{L(1 - \varepsilon)}{\rho_a D \varepsilon^3} \right) \left(\frac{V_a \rho_a}{S_b} \cdot \frac{1}{3600} \right)^2 \quad (65)$$

Where:

ε : bed porosity [-]

Re : Reynolds number [-]

L : bed thickness [m]

ρ_a : air density [kg m^{-3}]

D : average particles diameter [m]

S_b : bed section [m^2]

V_a : air velocity [m s^{-1}]

Pressure drops depends on many factors both structural and functional. In fact the structure, if the battery section crossed by the air flow, influences pressure drops; also the presence of fins and tubes are determinant. Another important structural quality is the bed thickness and consequently the amount of silica gel grains. Instead functional factors are for example the air velocity and so the air flow rate, the temperature of the air stream and so its density and so on. In the following plot

is reported the dependence of pressure drops from air flow rate for different values of porosity:

$\epsilon 1$	$\epsilon 2$	$\epsilon 3$	$\epsilon 4$	$\epsilon 5$
0,432	0,538	0,508	0,466	0,390

Table 16 – Porosity values utilized for the analysis

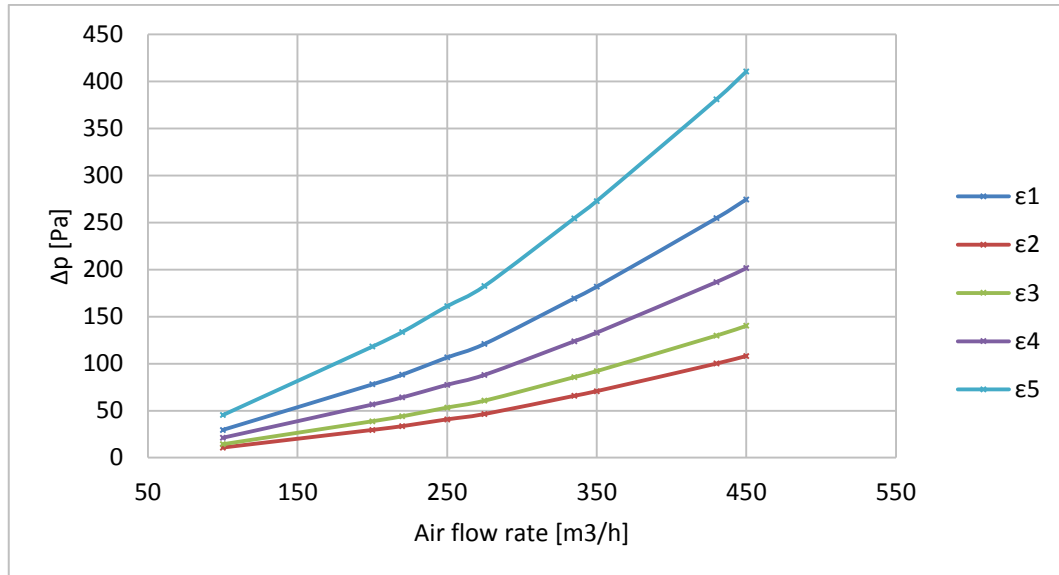


Figure 51 – Pressure drops of the silica gel battery in function of air flow rate

The highest curves correspond to the minimum porosity, so for the maximum density of grains, while the bottom curves correspond to the maximum porosity. Obviously higher the air flow higher the pressure drops. This is more evident with a similar graph that shows the pressure drops with the porosity variation (Figure 52).

Q1 [m3/h]	Q2 [m3/h]	Q3 [m3/h]	Q4 [m3/h]
100	220	335	430

Table 17 – Different flow rates used

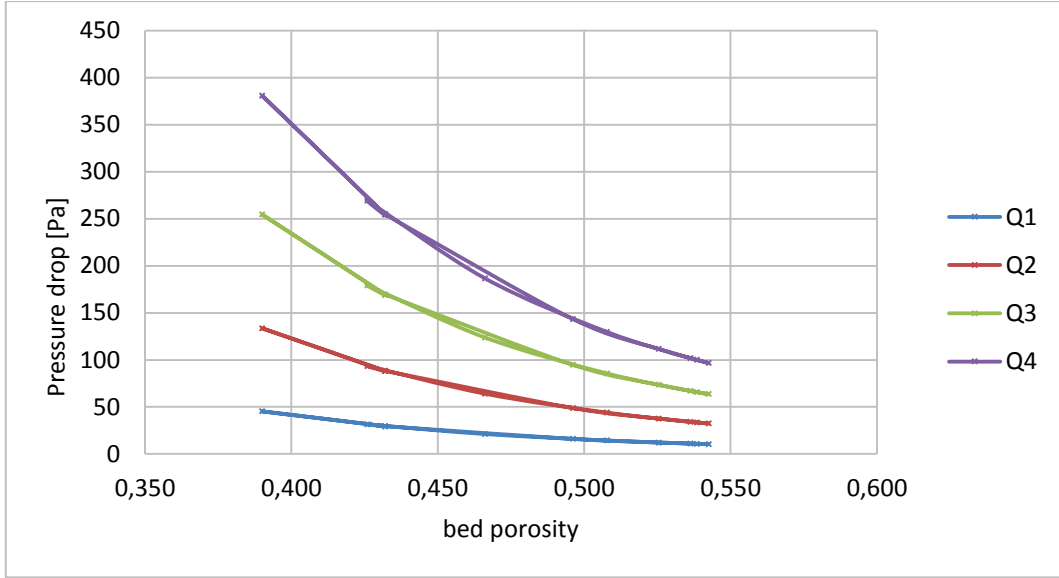


Figure 52 – Pressure drops of the silica gel battery in function of bed porosity

In conclusion a relation between pressure drops and exchange surface is investigated. As already said before the silica gel grains are idealized as regular spheres with the same diameter. So during the evaluation the sphere equations for surface and volume are used. The analysis takes into account also of the tubes and fins occupied volume. Here are show the equations used (see Table 5 – Battery dimensions):

$$V_t = \frac{\pi d_t^2}{4} \cdot L \cdot N_t \quad (65)$$

$$V_{fin} = L \cdot D \cdot \delta_{fin} \cdot N_{fin} \quad (66)$$

$$V_n = L \cdot D \cdot H - V_t - V_{fin} \quad (67)$$

$$V_{SiO_2} = V_n \cdot (1 - \varepsilon) \quad (68)$$

$$N_p = \frac{V_{SiO_2}}{V_p} \quad (69)$$

$$S_{ex} = N_p \cdot 4\pi R_p^2 \quad (70)$$

The values are reported in the following table:

Q1		Q2		Q3		Q4	
S ex (m2)	ΔP						
33,18	88,64	33,18	92,52	33,18	81,98	33,18	107,10
29,44	49,03	29,44	51,18	29,44	45,24	29,44	59,36
27,73	37,83	27,73	39,49	27,73	34,86	27,73	45,85
26,97	33,75	26,97	35,24	26,97	31,09	26,97	40,93
26,73	32,60	26,73	34,04	26,73	30,02	26,73	39,54
27,09	34,41	27,09	35,93	27,09	31,69	27,09	41,72
28,76	44,21	28,76	46,16	28,76	40,77	28,76	53,55
31,19	64,39	31,19	67,21	31,19	59,48	31,19	77,88
33,54	93,92	33,54	98,03	33,54	86,88	33,54	113,45
33,18	88,64	33,18	92,52	33,18	81,98	33,18	107,10
35,64	134,11	35,64	139,97	35,64	124,22	35,64	161,83
33,18	88,64	33,18	92,52	33,18	81,98	33,18	107,10

Table 18 – Data of Fig.51

The corresponding plot is the following:

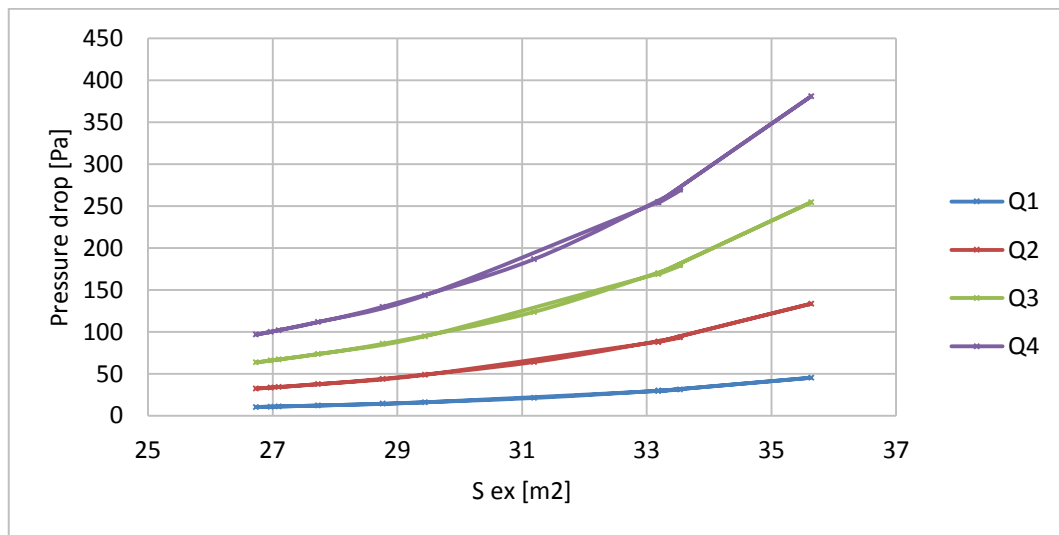


Figure 53 – Pressure drops of silica gel battery in funtion of exchange surface

Concerning coated zeolite from experimental data is possible to formulate equations of pressure drops of the battery for different air temperatures. Data are taken from a previous study done on the same adsorption system. In the following figure are reported the results:

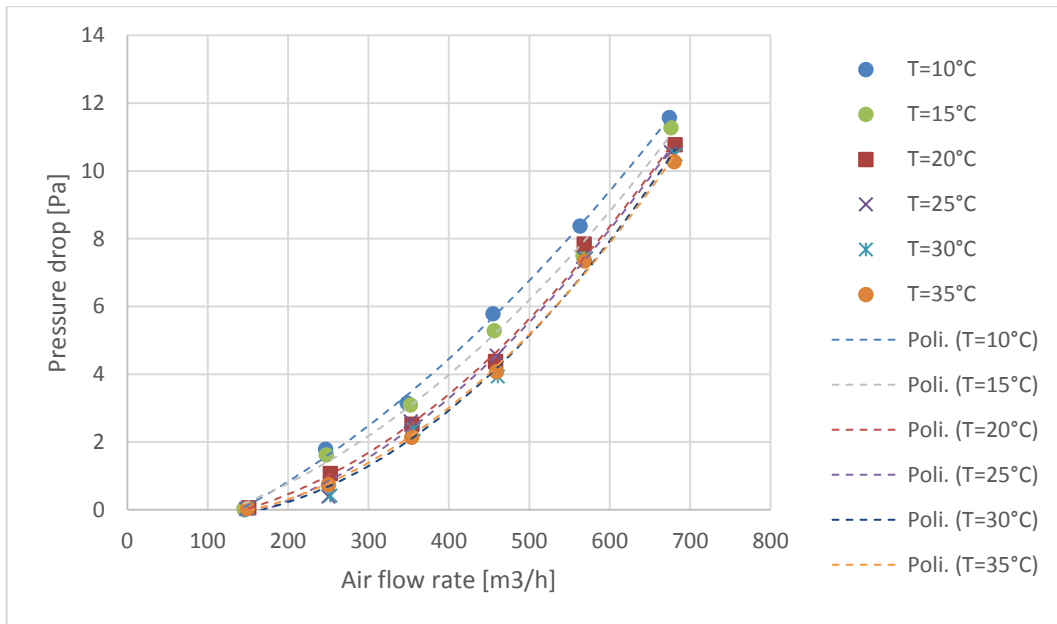


Figure 54 – Prssure drops of zeolite battery in function of air flow rate

The equation of interpolation lines is:

$$y = a \cdot x^2 + b \cdot x - c \quad (71)$$

With:

	a	b	c
Poli.(T=10°C)	0,00001654	0,0082	1,468804
Poli.(T=15°C)	0,00002027	0,003859	0,801743
Poli.(T=20°C)	0,00002487	-0,00015	0,505912
Poli.(T=25°C)	0,00002446	0,000415	0,786142
Poli.(T=30°C)	0,00002871	-0,0037	0,182217
Poli.(T=35°C)	0,00002702	-0,00269	0,234619

Table 19 – Data of Fig.52

It is possible to see that for the coated zeolite, pressure drops are sensible lesser than silica gel. This is due to the different porosity of the battery, in fact the coated layer does not fill the battery fins structure. However is important remember that the energy demand for the fun functioning is very lower respect to the pump energy demand.

4.4 Data analysis

In this section data acquired from the laboratory experiments are reported and elaborated to carry out the results of the study. The following figure shows the difference in humidity ratio between inlet and outlet during adsorption process for different air flow rate:

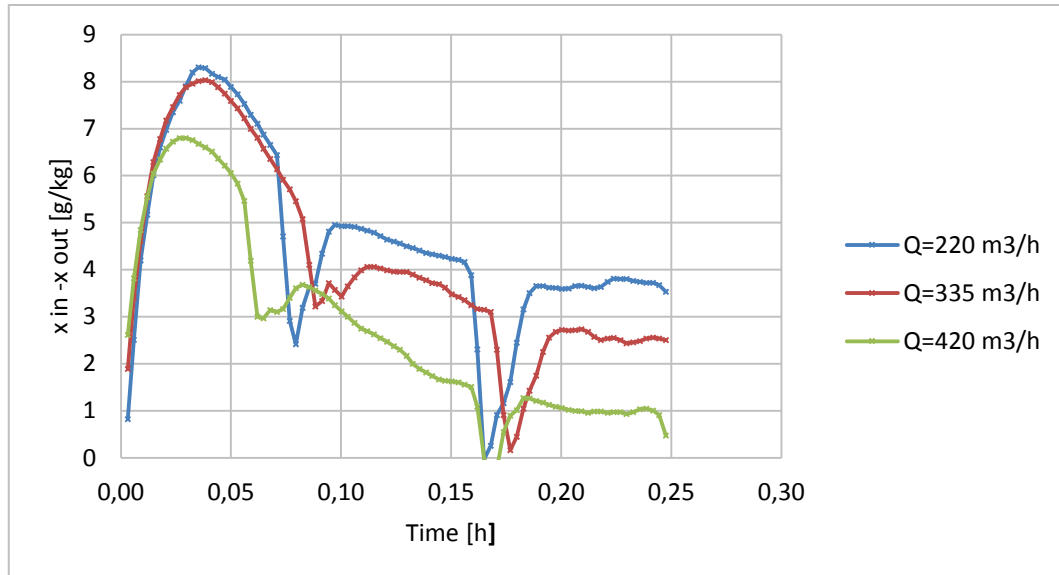


Figure 55 – Humidity difference between inlet and outlet during the adsorption

Lower peaks are due to a problem with the UTA humidifier that cause some problem for the correct performance of the tests. The humidifier shut down periodically falling down the air humidity values and causing a stop of the air providing blocking the UTA; the restart of the air flow is almost instantaneous while the humidifier take some time to re-boil water. In the following table is possible to see the exact moment of the shutdown of the humidifier:

	Time [h]	
Test-1	0,08	0,16
Test-2	0,09	0,18
Test-3	0,06	0,17

Table 20 – Time when the UTA humidifier shuts down

Nevertheless is possible to carry on a study about phenomena. It is possible to see how the highest ratio is correlated to the lower air flow; this happens perhaps because the adsorption process is favorited with an higher time of permanence of water vapour over the adsorption material. At the end of adsorption phase the three curves go to zero and in particular that one with the highest air flow goes to zero more rapidly.

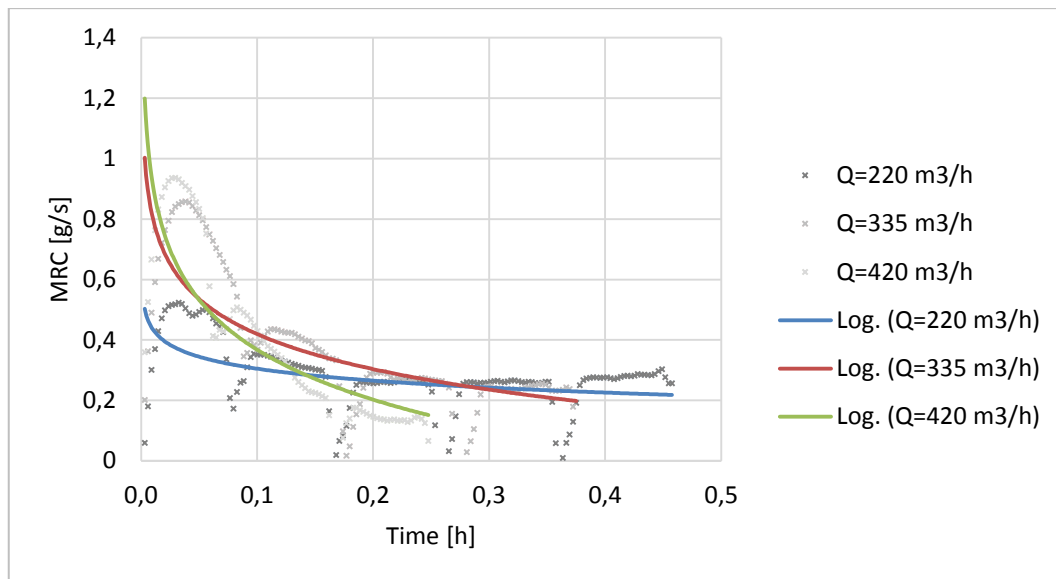


Figure 56 – MRC parameter during adsorption

It is possible to see how the MRC parameter varies with the increase of the air flow (Figure 56). The trend curves have a logarithm behaviour and the highest curve correspond to the highest air flow rate while the lowest with the lowest air flow rate. It is also possible view that with lower air flows, curves don't go to zero. This means that the battery was just able to adsorb more water vapour. With the highest air flow the curve go to zero more rapidly; consequently with higher air flow the adsorbent phase duration is lower.

In the following table are reported the results of exergy analysis for the three experiments.

Experiment	t ads [min]	t reg [min]	Q ads [kJ]	Q reg [kJ]	COP th	E el [kJ]	COP el	eta
Test 1	27	29	1778,07	1389,96	1,28	68,98	25,78	0,29
Test 2	23	25	1827,60	1513,74	1,21	60,99	29,96	0,26
Test 3	15	22	1343,28	1166,29	1,15	54,56	24,62	0,30

Table 21 – Final results of experiment

Duration time between adsorption and desorption are quite the same. Also the heat of adsorption and the heat provided for regeneration are quite the same (theoretically they should be equal). The electric energy needed for the process are very low influenced by different air flow rate; this because the fun consumption is very lower than water pump works, in fact the difference is

influenced by the functional time. The electric COP is higher than previous works ([9]) because the cooling process optimizes the system. It is possible to see how the efficiency of second law are quite the same for the all three experiments. This is an interesting results because permit to concentrate the system optimization on other parameters. Rather became more important to find an air flow that guarantee a useful adsorption duration for a real application. In the following figure is reported the heat pump process on the psychrometric diagram:

	Point	T dry [°C]	RH [%]	Twb [°C]	T dew [°C]	X [g/kg]	Ps [Pa]	h [kJ/kg]	rho [kg/m3]
Inlet condition	1	30	70	25,6	23,9	18,8	4250	78,1	1,165
Cooling	2	24	100	24,0	24,0	18,8	2987	72,1	1,189
Dehumidification	3	14	100	14,0	14,0	10,0	1600	39,2	1,230

Table 22 – Data of Fig.55

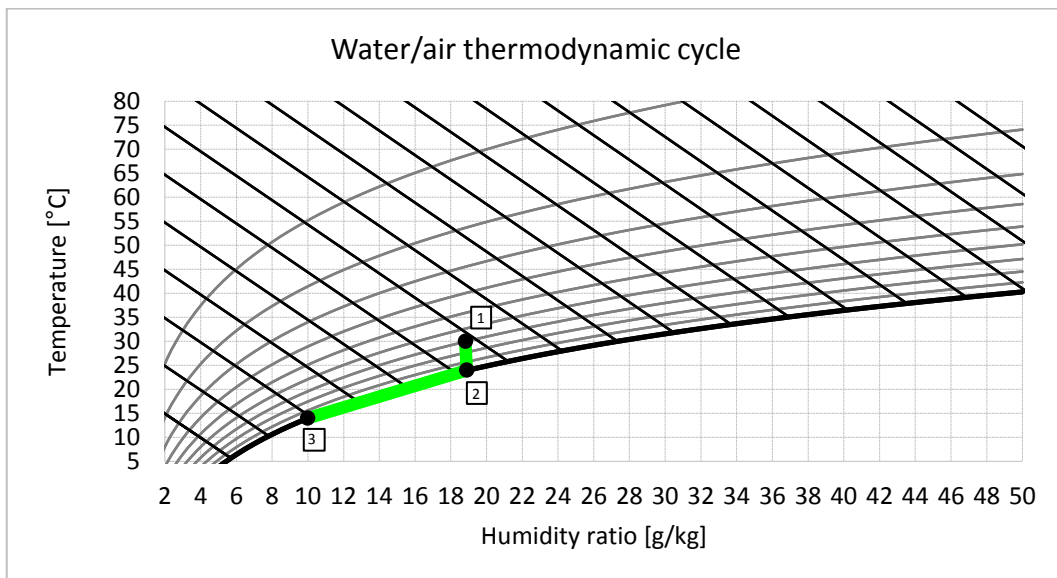


Figure 57 – Psicrometric cicle of the heat pump

The first transformation is a cooling without dehumidification. The cooling process brings the air stream up to the condensation point; here the relative humidity is about even 100%. Than starts the condensation of water vapour until to the desired value. In a real application there would be the post heating process to bring the air stream from about 14 °C to the desired temperature (e.g. 24 °C).

In the following table are reported results of the analysis of an hypothetical heat pump functioning under the same conditions of the adsorbent wall:

	Q [kW]	W [kW]	COP	eta
Heat pump 1st case	2,46	1,23	2,00	0,15
Heat pump 2nd case	2,46	0,98	2,50	0,18
Heat pump 3rd case	2,46	0,82	3,00	0,22

Table 23 – Final result for the heat pump

The heat pump studied must do the same transformation (dehumidification) of the adsorption system, then three different COP values are supposed and then the second principle efficiencies are evaluated. It possible to see that the best value of COP is lower than the adsorption system COP. It Is important remember that the air in output from the heat pump transformation is not ready to send to the conditioned space in fact the air stream exits at 14 °C and reasonably a heating is needed. Results show that from an exergy point of view the adsorption system is comparable with a traditional heat pump; in particular it is better. This means that for the development of this technology the study can focus on other parameter like processed air quality, adsorption autonomy, phases synchronization, payback time and economic analysis.

5 CONCLUSIONS

DEC systems are an interesting possibility of thermal utilization of solar source for solar cooling applications. Main benefits of this technology are the lower temperature required for regeneration compared with other systems like absorption chiller. Two different solutions of adsorption heat exchanger are here studied, with two different adsorbent materials: Silica gel and Zeolite SAPO-34.

The Silica gel is used in pseudo-spherical granular form, filling a finned coil heat exchanger obtaining a packed bed configuration. Instead in the second configuration a powder of Zeolite SAPO-34 cover a similar finned coil heat exchanger, creating an adsorption layer on the heat exchanger surfaces. The two configurations were tested in laboratories of Energy Department of Politecnico di Torino. A test rig for the realization of adsorption and regeneration tests in cooling mode it has been designed and realized in order to evaluate performances of the two configurations. Data logging it has been realized using the DAQ System interfaced with the Labview platform, in order to have a continuous monitor of the experiments. Particular attention was devoted for the realization of the data logging/monitoring chain starting from the calibration of sensors up to the electrical configuration of the DAQ system. The two configurations aim to test two different adsorption heat exchanger concepts: zeolite coated layer and silica gel grains. In particular the test is focused on the former application. The differences in adsorbent structure and application leads to a substantially decrease in mass of adsorbent; this is a very interesting result considering that the lightness and compactness are two important behaviour of future adsorption systems. The lightness is payed with a less amount of useful surface for adsorption interaction and consequently with a less phases duration. This is highlighted by the experiments and in particular by the comparison with the old test with silica gel grains; that experiment has a duration time of some hours while tests with zeolite battery have a duration time more or less of half hour. As expected pressure drops are very lower with thin layer battery than silica gel battery, but this is not a fundament penalization because the fun work is in essence negligible respect to the circulate pump work; this is clear since the space between fins is not filled with adsorbent material. It also important reports that the electric energy consumption is lower with the adsorption system than a classical heat pump;

excluding the fan work, the only electricity consumption is due to the circulation pump (40 W) while for the heat pump configuration is due to the compressor work (800 W with a COP of 3). An important optimization that is studied in this work is the cooling of the battery during the adsorption phase, to increase and favour the adsorption process; this configuration has to be developed in order to become available also in a real application. From the study merged that is important chose the most fitting air flow rate; in fact with a too high flow rate adsorption is not promoted. From the literature is possible to conclude that zeolite has better performances from an adsorption point of view than silica gel, but it is a more complex technology. In fact the thin layer on the battery fins is difficult to realize and makes it delicate and difficult to repair when it fails. Silica gel is a simpler and more tested technology. From a performance point of view zeolite has higher rate of adsorption but is more difficult to regenerate due to the more powerful bond between sorbate and adsorbent. In fact the second principle efficiency is better. In a real application a storage system for cooling water must be performed; this because the cooling process needs an high water flow. In this case a pump work has to be considered also for adsorption process lowering the efficiency.

6 BIBLIOGRAPHY

- [1] C. Pouil-, “Biography: Augustin Bernard Mouchot (1825-1912) Biography: Augustin Bernard Mouchot Biography: Augustin Bernard Mouchot,” no. August 1866, pp. 1–3, 1912.
- [2] N. Subramanyam, M. P. Maiya, and S. S. Murthy, “Application of desiccant wheel to control humidity in air-conditioning systems,” *Appl. Therm. Eng.*, vol. 24, no. 17–18, pp. 2777–2788, 2004.
- [3] D. S. Kim and C. A. Infante Ferreira, “Solar refrigeration options - a state-of-the-art review,” *Int. J. Refrig.*, vol. 31, no. 1, pp. 3–15, 2008.
- [4] F. M. Montagnino, “Solar cooling technologies. Design, application and performance of existing projects,” *Sol. Energy*, vol. 154, pp. 144–157, 2016.
- [5] Federation European Solar Thermal Industry, “Solar Assisted Cooling, State of the Art,” *Key Issues Renew. Heat Eur.*, p. 21, 2006.
- [6] P. Finocchiaro, M. Beccali, and V. Gentile, “Experimental results on adsorption beds for air dehumidification,” *Int. J. Refrig.*, vol. 63, pp. 100–112, 2016.
- [7] M. Beccali, P. Finocchiaro, and B. Nocke, “Energy performance evaluation of a demo solar desiccant cooling system with heat recovery for the regeneration of the adsorption material,” *Renew. Energy*, vol. 44, pp. 40–52, 2012.
- [8] P. Finocchiaro, M. Beccali, and B. Nocke, “Advanced solar assisted desiccant and evaporative cooling system equipped with wet heat exchangers,” *Sol. Energy*, vol. 86, no. 1, pp. 608–618, 2012.
- [9] M. Simonetti, G. Chiesa, M. Grosso, and G. V. Fracastoro, “NAC wall: An open cycle solar-DEC with naturally driven ventilation,” *Energy Build.*, vol. 129, pp. 357–366, 2016.
- [10] M. Simonetti, V. Gentile, G. V. Fracastoro, A. Freni, L. Calabrese, and G. Chiesa, “Experimental testing of the buoyant functioning of a coil coated with SAPO34 zeolite, designed for solar DEC (Desiccant Evaporative Cooling) systems of buildings with natural ventilation,” *Appl. Therm. Eng.*, vol. 103, pp. 781–789, 2016.
- [11] P. Finocchiaro, M. Beccali, V. Lo Brano, and V. Gentile, “Monitoring Results and Energy Performances Evaluation of Frescoo Solar DEC Systems,” *Energy Procedia*, vol. 91, pp. 752–758, 2016.
- [12] M. Simonetti, V. Gentile, L. Liggieri, G. V. Fracastoro, and M. G. Carrabba, “Experimental analysis of ‘NAC-wall’ for hybrid ventilation mode,” *Energy Build.*, vol. 152, pp. 399–408, 2017.
- [13] D.M.Ruthven, “Principles of adsorption & adsorption process.”
- [14] L. Pistocchini, S. Garone, and M. Motta, “Air dehumidification by cooled adsorption in silica gel grains. Part II: Theoretical analysis of the prototype

- testing results," *Appl. Therm. Eng.*, vol. 110, pp. 1682–1689, 2017.
- [15] N. Arnold and D. Ovenden, "REPTILES & AMPHIBIANS."
- [16] A. Freni, G. Maggio, F. Cipitì, and Y. I. Aristov, "Simulation of water sorption dynamics in adsorption chillers: One, two and four layers of loose silica grains," *Appl. Therm. Eng.*, vol. 44, pp. 69–77, 2012.
- [17] D. Cheng, E. A. J. F. (Frank) Peters, and J. A. M. (Hans) Kuipers, "Performance study of heat and mass transfer in an adsorption process by numerical simulation," *Chem. Eng. Sci.*, vol. 160, no. November 2016, pp. 335–345, 2017.
- [18] T. Dell and A. Umida, "Termodinamica dell'aria umida 5.1," pp. 1–16.
- [19] M. Kanoğlu, M. Ö. Çarpınlioğlu, and M. Yildirim, "Energy and exergy analyses of an experimental open-cycle desiccant cooling system," *Appl. Therm. Eng.*, vol. 24, no. 5–6, pp. 919–932, 2004.
- [20] A. Koca, H. F. Oztop, T. Koyun, and Y. Varol, "Energy and exergy analysis of a latent heat storage system with phase change material for a solar collector," *Renew. Energy*, vol. 33, no. 4, pp. 567–574, 2008.
- [21] T. Zhang, X. Liu, J. Liu, H. Tang, and Y. Jiang, "Exergy and entransy analyses in air-conditioning system part 2—Humid air handling process," *Energy Build.*, vol. 139, pp. 10–21, 2017.
- [22] A. Bejan, *Advanced Engineering Thermodynamics*. 2006.
- [23] M. M. Rafique, P. Gandhidasan, H. M. S. Bahaidarah, and M. A. Shakir, "Thermal and exergetic performance evaluation of an absorption type desiccant dehumidifier," *Environ. Prog. Sustain. Energy*, vol. 0, no. 0, pp. 1–13, 2017.
- [24] B. Eisfeld and K. Schnitzlein, "The influence of confining walls on the pressure drop in packed beds," *Chem. Eng. Sci.*, vol. 56, no. 14, pp. 4321–4329, 2001.
- [25] L. Pistocchini, S. Garone, and M. Motta, "Porosity and pressure drop in packed beds of spheres between narrow parallel walls," *Chem. Eng. J.*, vol. 284, pp. 802–811, 2016.

7 WEBLIOGRAPHY FOR FIGURES

- www.simonsboiler.com.au
- www.cliquesolar.com Source ESTIF , Key Issues for Renewable Heat in Europe, August 2006
- www.joules-project.eu
- www.wikipedia.org By Michael Schmid (Drawing created by myself)
- www.biologists.org
- www.ofrioquevemdosol.blogspot.it 201109solar-refrigeration.html
- www.commonswikimedia.org
wikiFileSchematic_silica_gel_surface.png.2
- www.mskcc.org
- www.researchgate.net
- www.appuntimania.com
- www.oorja.in

Summary of figures

Figure 1 – Universal Exhibition in Paris (1878).....	1
Figure 2 – Time variations of the solar radiation and demands of refrigeration and heating. (source: www.ofrioquevemdosol.blogspot.it).....	2
Figure 3 – Scheme of a thermally driven chiller	3
Figure 4 – Absorption process (source: ESTIF, key issues for renewable heat in Europe. August 2006)	5
Figure 5 – Absorption process	5
Figure 6 – Adsorption process	6
Figure 7 – Open cycle solar DEC	8
Figure 8 – Open cycle solar DEC with two additional coil	8
Figure 9 – Open cycle solar DEC with two wet heat exchangers.....	9
Figure 10 – Air to air heat exchanger (source: Recuperator).....	9
Figure 11 – Evaporative cooling.....	10
Figure 12 – NADEH wall	11
Figure 13 – Adsorption isotherms proposed by Brunauer	15
Figure 14 – Scheme of inversion temperature	17
Figure 15 – Toes and setae of gecko.....	19
Figure 16 – Lennard-Jones potential	21
Figure 17 – Molecular structure and isotherms of silica gel.....	23
Figure 18 – Molecular structure and isotherms of zeolite.....	24
Figure 19 – Rotating wheel with honeycomb structure	24
Figure 20 – Scheme of adsorption/desorption system control volume.....	27
Figure 21 – Physical exergy in function of temperature.....	32
Figure 22 – Chemical exergy in function of moisture quantity	32
Figure 23 – Specific exergy variation with the temperature.....	34
Figure 24 – Scheme of a heat pump	36

Figure 25 – System general scheme	39
Figure 26 – Solar collectors on the roof of the laboratory.....	39
Figure 27 – Adsorption and regeneration process on the battery	40
Figure 28 – Water tank and water pump of the secondary loop	41
Figure 29 – UTA.....	42
Figure 30 – Structure of the two batteries.....	42
Figure 31 – Silica gel battery	43
Figure 32 – Zeolite battery.....	44
Figure 33 – Particular of the adsorbent material. On the left silica gel while on the right zeolite	44
Figure 34 – Banking of silica gel grains	45
Figure 35 – Cracking of zeolite layer	45
Figure 36 – Cooling connections	46
Figure 37 – Control panel scheme	47
Figure 38 – Sensors scheme.....	47
Figure 39 – Sensors position on the wall.....	48
Figure 40 – STD 100-50 calibration curve	51
Figure 41 – STD 100-300 calibration curve	51
Figure 42 – Pt100 calibration curve.....	53
Figure 43 – Test-1: adsorption and regeneration with an air stream of 220 m ³ /h .	56
Figure 44 – Test-2: adsorption and regeneration with an air stream of 335 m ³ /h .	57
Figure 45 – Test-3: adsorption and regeneration with an air stream of 430 m ³ /h .	57
Figure 46 – Thermal power on air during adsorption/regeneration process.....	58
Figure 47 – Electric power consumption during the adsorption/regeneration experiment	59
Figure 48 – Silica gel test (old experiment).....	60
Figure 49 – Molecular structure of different package	61

Figure 50 – The correlation between porosity and fins dimensions for the silica gel battery	63
Figure 51 – Pressure drops of the silica gel battery in function of air flow rate....	64
Figure 52 – Pressure drops of the silica gel battery in function of bed porosity ...	65
Figure 53 – Pressure drops of silica gel battery in funtion of exchange surface ...	66
Figure 54 – Prsssure drops of zeolite battery in function of air flow rate	67
Figure 55 – Humidity difference between inlet and outlet during the adsorption.	68
Figure 56 – MRC parameter during adsorption.....	69
Figure 57 – Psicrometric cicle of the heat pump	70

Summary of tables

Table 1 – Parameters for saturation pressure experimental curves	29
Table 2 – Dead state.....	32
Table 3 – Parameters of humidity used for the study in table 4	33
Table 4 – Data for Fig.23	34
Table 5 – Battery dimensions	42
Table 6 – Experimental results of NTC sensors	50
Table 7 – Experimental results of Pt100.....	52
Table 8 – STD 100-50 curve parameters	53
Table 9 – STD 100-300 curve parameters	53
Table 10 – Pt100 curve parameters.....	54
Table 11 – Functional hypothesis	56
Table 12 – Heat flux exchanged	58
Table 13 – Electric consumption	59
Table 14 – Dimension of fins	62
Table 15 – Results.....	62
Table 16 – Porosity values utilized for the analysis	64
Table 17 – Different flow rates used	64
Table 18 – Data of Fig.51	66
Table 19 – Data of Fig.52	67
Table 20 – Time when the UTA humidifier shuts down	68
Table 21 – Final results of experiment	69
Table 22 – Data of Fig.55	70
Table 23 – Final result for the heat pump.....	71